



# NATIONAL ADVISORY COMMITTEE FOR AERONAUTICS

TECHNICAL NOTE 3047

IMPINGEMENT OF WATER DROPLETS ON NACA 65A004 AIRFOIL  
AND EFFECT OF CHANGE IN AIRFOIL THICKNESS FROM  
12 TO 4 PERCENT AT 4° ANGLE OF ATTACK

By Rinaldo J. Brun, Helen M. Gallagher  
and Dorothea E. Vogt

Lewis Flight Propulsion Laboratory  
Cleveland, Ohio



Washington  
November 1953

AFMDC  
TECHNICAL LIBRARY



0066122

NATIONAL ADVISORY COMMITTEE FOR AERONAUTICS

## TECHNICAL NOTE 3047

IMPINGEMENT OF WATER DROPLETS ON NACA 65A004 AIRFOIL AND EFFECT OF  
CHANGE IN AIRFOIL THICKNESS FROM 12 TO 4 PERCENT AT  
 $4^{\circ}$  ANGLE OF ATTACK

9262

By Rinaldo J. Brun, Helen M. Gallagher, and Dorothea E. Vogt

## SUMMARY

CT-1

The trajectories of droplets in the air flowing past an NACA 65A004 airfoil at an angle of attack of  $4^{\circ}$  were determined. The amount of water in droplet form impinging on the airfoil, the area of droplet impingement, and the rate of droplet impingement per unit area on the airfoil surface were calculated from the trajectories and presented to cover a large range of flight and atmospheric conditions.

The effect of a change in airfoil thickness from 12 to 4 percent at  $4^{\circ}$  angle of attack is presented by comparing the impingement calculations for the NACA 65A004 airfoil with those for the NACA 65<sub>1</sub>-208 and 65<sub>1</sub>-212 airfoils. The rearward limit of impingement on the upper surface decreases as the airfoil thickness decreases. The rearward limit of impingement on the lower surface increases with a decrease in airfoil thickness. The total water intercepted decreases as the airfoil thickness is decreased.

## INTRODUCTION

Recent developments in high-speed aircraft necessitate an appraisal of the icing problem for low-drag airfoils, and particularly for thin airfoils. A study of the impingement of cloud droplets, similar to that presented in reference 1 for a 12- and an 8-percent-thick low-drag airfoil, is presented herein for a 4-percent-thick airfoil. The results discussed in the reference cited apply to NACA 65<sub>1</sub>-212 and 65<sub>1</sub>-208 airfoils. The data presented in reference 1 and the present study permit the determination of the amount of water in droplet form impinging on the airfoils, the extent of impingement on the airfoil surface, and the rate of water impingement per unit area of the airfoil surface. The calculations apply at an angle of attack of  $4^{\circ}$ .

The NACA 65-series airfoil sections were chosen for icing analysis, because these sections are particularly adaptable to airplanes having high level-flight speeds. The airfoils for which impingement data are presented in reference 1 are adaptable to high-speed subsonic transport and cargo airplanes. Although an angle of attack of  $4^{\circ}$  may be somewhat greater than required for most cruising conditions, it is representative for an aircraft with those airfoils operating under conditions giving a relatively large area of droplet impingement on the airfoil. The 4-percent-thick airfoil, for which impingement data are presented herein, is adaptable to high-speed subsonic, transonic, and low-supersonic airplanes, particularly fighter-type aircraft. An angle of attack of  $4^{\circ}$  is greater than the usual cruise attitude for pursuit or fighter-type airplanes; however, this value is not an extreme maximum for hovering, landing, and some types of flight plans. The choice of  $4^{\circ}$  for the angle of attack permits an extension of previous studies on effect of thickness ratio on droplet impingement to a 4-percent-thick airfoil section. In general, this extension is useful even though the shape of the mean line of the NACA 65A004 airfoil is slightly different from that of the other two airfoils, because changes in the impingement characteristics due to differences in airfoil shape associated with differences in the mean line usually are less than impingement changes caused by a change in thickness ratio. These effects are discussed as the impingement data are presented. The analysis of droplet impingement on the NACA 65A004 airfoil was made at the NACA Lewis laboratory. The results are applicable under the following conditions: chord lengths from 2 to 20 feet; altitudes from 1000 to 35,000 feet; airplane speeds from 150 miles per hour to the flight critical Mach number; and droplet diameters from 5 to 100 microns.

2956

#### SYMBOLS

The following symbols are used in this report:

- d droplet diameter, microns (micron =  $3.28 \times 10^{-6}$  ft)
- K inertia parameter,  $1.704 \times 10^{-12} \frac{d^2 U}{\mu L}$ , dimensionless
- L airfoil chord length, ft
- $Re_0$  free-stream Reynolds number with respect to droplet,  $4.813 \times 10^{-6} \frac{d \rho_a U}{\mu}$ , dimensionless
- S distance on surface of airfoil measured from point of intersection of geometric chord line with airfoil leading edge, ratio to chord length

9562  
CI-1 back

$t$  airfoil thickness, ratio to chord length  
 $U$  flight speed, mph  
 $u$  local air velocity, ratio to free-stream velocity  
 $W$  rate of water impingement per unit span of airfoil, lb/(hr)(ft span)  
 $W_\beta$  local rate of water impingement, lb/(hr)(sq ft)  
 $w$  liquid-water content in cloud, g/cu m  
 $x, y$  rectangular coordinates, ratio to chord length  
 $x'$  distance parallel to geometric chord line measured from leading-edge chord point, ratio to chord length  
 $y'$  distance measured perpendicular to  $x'$ , ratio to chord length  
 $\beta$  local impingement efficiency,  $\frac{dy_0}{ds}$ , dimensionless  
 $\mu$  viscosity of air, slugs/(ft)(sec)  
 $\rho$  density, slugs/cu ft

**Subscripts:**

$a$  air  
 $l$  lower airfoil surface  
 $m$  total  
 $s$  airfoil surface  
 $u$  upper airfoil surface  
 $0$  free stream

#### IMPINGEMENT OF DROPLETS ON NACA 65A004 AIRFOIL

In order to obtain the extent of impingement and the rate of droplet impingement per unit area on the airfoil, the cloud droplet trajectories with respect to the airfoil were determined. The method for calculating

2956

the droplet trajectories is described in reference 1. A solution of the differential equations that describe the droplet motion was obtained with the use of the mechanical analog (described in ref. 2) based on the principle of a differential analyzer. The air-flow field around the airfoil was obtained by the vortex substitution method described in reference 1, with the exception that for the NACA 65A004 airfoil the velocities at the surface of the airfoil as given in reference 1 were calculated by the method described in reference 3; whereas the surface velocities on the 65<sub>1</sub>-212 and 65<sub>1</sub>-208 airfoils were obtained from wind-tunnel measurements of the pressure coefficients. The values of the surface velocities for the 65A004 airfoil were furnished to the Lewis laboratory by the Douglas Aircraft Corporation (see fig. 1). Although the droplet trajectories were calculated for an incompressible flow field, the results of the calculations can be applied up to the flight critical Mach number (ref. 4).

The geometric chord line of the airfoil is oriented at an angle of 4° with the x-axis of the rectangular coordinate system, and the leading edge is placed at the origin of the coordinates, as shown in figure 2. The airfoil orientation presented in reference 1 is retained herein. At an infinite distance ahead of the airfoil, the uniform air flow carrying the cloud droplets is assumed to be approaching the airfoil from the negative x-direction and parallel to the x-axis. All distances are dimensionless, because they are ratios of the respective actual distances to the airfoil chord length L.

#### Rate of Water Interception

The rate of total water interception, in pounds per hour per foot of wing span, is determined by the tangent droplet trajectories (fig. 2), by the speed of the aircraft, and by the liquid-water content in the cloud. The flight speed and size of the airfoil, as well as the droplet size in the cloud, are the principal variables that affect the spacing between the two tangent trajectories. The amount of water that strikes the airfoil is proportional to the spacing  $y_{0,u} - y_{0,l}$ , and the rate of total water interception per unit span of the airfoil on that portion of the airfoil surface bounded by the upper and lower tangent trajectories can be calculated from the relation

$$W_m = 0.33(y_{0,u} - y_{0,l})LU_w \quad (1)$$

The values of  $y_{0,u} - y_{0,l}$  are given in figure 3 in terms of the reciprocal of the inertia parameter and the free-stream Reynolds number. The inertia parameter K is a measure of the droplet size, the flight speed and size of the airfoil, and the viscosity of the air, through the relation

$$K = 1.704 \times 10^{-12} \frac{d^2 U}{\mu L} \quad (2)$$

The free-stream Reynolds number is defined with respect to the droplet size as

$$Re_0 = 4.813 \times 10^{-6} \frac{d \rho_a U}{\mu} \quad (3)$$

2935

A graphical procedure for determining values of the dimensionless parameters  $K$  and  $Re_0$  in terms of airplane speed, chord length, altitude, and droplet size is presented in appendix B of reference 1.

The variation of rate of water interception with airfoil speed is summarized for an altitude of 20,000 feet in figure 4, in which the ordinate  $W_m/w$  is the total rate of water impingement per foot span of airfoil per unit liquid-water content (g/cu m) in the cloud. Several chord lengths ranging in value from 2 to 20 feet were considered. The values in figure 4 are for flight through a uniform cloud composed of droplets 15, 20, 30, and 40 microns in diameter. The values of  $W_m$  in figure 4 are based on the most probable icing temperature as a function of altitude presented in figure 15 of reference 1. (The most probable icing temperature was obtained from approximately 300 icing observations in flights.) As shown in reference 1, a change in altitude of 10,000 feet will change the rate of water impingement by approximately 7 percent. The droplet size and the liquid-water content of clouds are seldom known with sufficient accuracy (ref. 2) to permit the rate of water impingement to be calculated within 10 percent; therefore, within practical limits of application, the results of figure 4 can be used over a wide range of altitudes (approx.  $\pm 10,000$  ft, see ref. 1).

The effect of wing taper can also be obtained from figure 4, provided that for each section of span considered the taper is small enough that two-dimensional flow over the section is approximated, as is mentioned in reference 1.

#### Extent of Impingement

The limit of impingement is determined by the point of tangency on the airfoil surface of the two tangent trajectories. The rearward limits of impingement on the upper surface are shown in figure 5(a), and on the lower surface in figure 5(b). The distances  $S_u$  and  $S_l$  are measured on the airfoil surface from the point of intersection of the geometric chord line with the leading edge (fig. 2) in terms of the chord length.

The limits of impingement are given in figure 5 in terms of the reciprocal of the inertia parameter and the free-stream Reynolds number; whereas, in figures 6 and 7, the limits are summarized for the same speeds, chord lengths, droplet sizes, and altitude given in figure 4. The limits on the upper surface are given in figure 6, and on the lower surface in figure 7. For any given combination of airfoil and droplet size and flight speed, the extent of impingement on the upper surface is much less than on the lower surface.

2936

### Impingement Distribution on Surface

Trajectory starting ordinate as function of point of impact. - The manner in which water is distributed on the surface of an airfoil can be obtained if the starting point of a droplet trajectory is known with respect to the point of impingement on the surface. The starting ordinate  $y_{0,u}$  at infinity of any impinging trajectory, including the upper and lower tangent trajectories (fig. 1), can be found in figure 8 with respect to the point of impingement on the surface. The values for the starting and ending positions of the trajectories are shown in figure 8 for three values of free-stream Reynolds number. For each value of  $Re_0$ , curves for several values of  $l/K$  are given.

The amount of water impinging between any two given points on the airfoil surface may be found by applying the results of figure 8 in the relation

$$W = 0.33UwL(y_{0,1} - y_{0,2}) \quad (4)$$

For example, the amount of water impinging between the -0.05 chord point and the -0.10 chord point on the surface of a 12.5-foot-chord airfoil traveling at 400 miles per hour at an altitude of 10,000 feet through a cloud composed of droplets 25 microns in diameter ( $l/K = 10$ ,  $Re_0 \approx 256$ ) can be found from equation (4) if the liquid-water content in the cloud is known. The values of  $y_{0,1}$  and  $y_{0,2}$  required in equation (4) are -0.071 and -0.075, respectively.

The values of  $y_{0,u} - y_{0,l}$  obtained from the end points of each curve in figure 8 are the same as the values given in figure 3. The value of  $y_{0,l}$  for  $l/K = 0$  (not shown in fig. 8) is -0.070 at  $S_l = 1.00229$  (airfoil trailing edge) for all values of  $Re_0$ .

Local impingement efficiency. - The local rate of droplet impingement per unit area of airfoil surface can be determined from the expression

$$w_\beta = 0.33U_w \frac{dy_0}{dS} = 0.33U_w\beta \quad .(5)$$

which is related to equation (4), with proper consideration for the fact that  $y_0$  and  $S$  are based on the wing chord  $L$ . The values of the local impingement efficiency  $\beta$  as a function of the airfoil distance  $S$  are given in figure 9. These values were obtained from the slopes of the curves in figure 8.

For all the conditions presented in figure 9, the maximum rate of local impingement occurs between  $S = -0.01$  and  $S = 0$ . Because of the geometry of the airfoil and the manner in which the droplets approach the airfoils in the neighborhood of the stagnation point, the curves in figure 8 are not well defined between  $S = -0.01$  and  $S = 0$ . Since the values of  $\beta$  are obtained from the slopes of the curves in figure 8, the maximum values of  $\beta$  in figure 9 also are subject to some question. The possible error in the maximum value of  $\beta$  is estimated to be  $\pm 25$  percent. As was discussed in reference 1, this possible error is not considered very serious, because only a small portion of the total water impinging on the airfoil requires redistribution if the maximum value of  $\beta$  is varied by as much as the maximum possible error.

The uncertainties in the values of  $\beta$  given in figure 9 for the thin, sharp-nosed NACA 65A004 airfoil are much greater than the uncertainties in the  $\beta$  values given in reference 2 for a cylinder, which is a blunt-nosed object. The values of  $\beta$  given in figure 9 are very sensitive to the shape of the curves in figure 8. Because of the geometry of the sharp-nosed NACA 65A004 airfoil and the manner in which the trajectories approach the airfoil surface, small errors in the calculated trajectories will result in considerable error in the slopes of the curves of figure 8. The random errors resulting from the errors in calculating the trajectories were probably reduced considerably in the  $\beta$  curves of figure 9 by fairing the curves as a consistent family of curves. The possible error in the values of  $\beta$  for surface positions other than near the stagnation point is estimated to be somewhat less than  $\pm 10$  percent. Since the total water impinging is directly related to

$$y_{0,u} - y_{0,l} = \int_{-S_l}^{S_u} \beta dS$$

the total area under the curves in figure 9 is determined by the curves of figure 3. If the requirement is imposed that the total area under the  $\beta$  curves of figure 9 cannot be altered, any judicious refairing of the  $\beta$  curves to account for uncertainties in the curves of figure 8 will redistribute only a small amount of the total water.

#### EFFECT OF AIRFOIL THICKNESS RATIO ON IMPINGEMENT OF DROPLETS

The comparison of impingement on an NACA 65<sub>1</sub>-212 airfoil with that on an NACA 65<sub>1</sub>-208 airfoil presented in reference 1 is extended herein to include the NACA 65A004 airfoil. The three airfoils are illustrated in figure 10, and the surface coordinate points are presented in table I. The comparison in this report emphasizes the effect of thickness ratio on droplet impingement. All three airfoils have substantially the same basic thickness form and all have the position of minimum pressure at the 50-percent-chord point. The principal difference is that the NACA 65A004 airfoil is a symmetrical airfoil for which the section has substantially straight lines for both the upper and lower surfaces from about 0.8 chord to the trailing edge; whereas the NACA 65<sub>1</sub>-212 and 65<sub>1</sub>-208 airfoils are both slightly cambered for a design lift coefficient of 0.2 and have points of slight inflection on the upper and lower surfaces near the trailing edge.

2936

Although a change in camber of an airfoil will result in a different air-flow field ahead of the airfoil, the small difference in mean camber line among the three airfoils being compared herein is considered to have only a slight effect on the droplet trajectories within the range of meteorological and flight conditions of usual interest. This consideration is based on the data presented in reference 5 on two 15-percent-thick Joukowski airfoils at zero angle of attack, but with differences in camber. One of the Joukowski airfoils is symmetrical, whereas the other is cambered with a mean camber line  $a = 1$  (see ref. 6 for listing of coordinate points for mean camber lines). For both Joukowski airfoils the total water impinging is substantially the same under all meteorological and flight conditions. Although some difference exists in the extent of impingement between the cambered and uncambered airfoils, the differences are largest when the comparison is made for combinations of large droplets and high speed than for combinations of small droplets and low speed. This comparison indicates that camber does not change the flow field ahead of the airfoil enough to influence the shape of the trajectories of small droplets at low speeds, which are associated with small values of  $K$  and more nearly follow the air streamlines than those associated with large values of  $K$ . The larger differences found in the comparison at the large values of  $K$  are due to differences in the physical shape of the two airfoils associated with the differences in the mean camber lines.

The manner in which the airfoil shape affects the extent of impingement is discussed further in the subsequent sections where the impingement characteristics of the NACA 65<sub>1</sub>-212, 65<sub>1</sub>-208, and 65A004 airfoils are compared. Most of the differences in impingement characteristics among the three airfoils are caused by differences in thickness ratio, because the thickness ratio is a principal variable defining the geometry of the airfoil and its attendant air velocity field.

29

CT-2

#### Basis of Comparison

The effect of airfoil thickness ratio on droplet impingement is illustrated with examples involving three airplanes using the three airfoils being considered. The physical conditions established permit the comparison of droplet impingement on the three airfoils of equal chord length on the three airplanes flying together at the same speed and altitude. These conditions are established at a constant speed of 400 miles per hour, a chord length of 12.5 feet, and an altitude of 10,000 feet (most probable icing temperature, ref. 1). The impingement on the three airfoils is compared at each of three widely separated values of  $1/K$ : 1, 10, and 100. For each value of  $1/K$  the cloud droplet size and free-stream Reynolds number are different, as shown in the following tabulation:

Reciprocal of inertia parameter, $1/K$	Droplet diameter, $d$ , microns	Free-stream Reynolds number, $Re_0$
1	80	793
10	25	254
100	8	79

The value of free-stream Reynolds number tabulated is the value obtained from equation (3) for the physical conditions established for this comparison.

#### Extent of Impingement

Upper surface. - The rearward limit of impingement on the upper surface decreases as the thickness ratio is decreased, as shown in figure 11. The limit of impingement should continue to decrease for thicknesses less

than 0.04 chord, because for a thin plate at  $4^\circ$  angle of attack the extent of impingement on the upper surface is zero. The rearward change of limit of impingement on the upper surface shown in figure 11 is all caused by the change in airfoil geometry associated with decrease in thickness ratio and is not due to a change in mean line among the airfoils, because impingement on the upper surface is confined to the vicinity of the leading edge where the airfoil shape is determined by the leading-edge radius (table I).

Lower surface. - For very small values of  $l/K$  ( $l/K < 1$ ) the extent of impingement is mainly influenced by the shape of the airfoil lower surface. Small values of  $l/K$  are associated with droplets with large momentum, that is, large in size and moving with high speed. The momentum of these droplets is so large that the trajectories are nearly straight lines and are not influenced appreciably by the air-flow field around the airfoil. For this reason, the tangency of these trajectories is greatly influenced by the physical shape and angle of attack of the airfoil. The lower-surface shape of the NACA 65<sub>1</sub>-212 and 65<sub>1</sub>-208 airfoils is such that at  $4^\circ$  angle of attack the extent of impingement is limited to  $S = -0.538$  chord and  $-0.654$  chord, respectively, for the extreme case of  $l/K = 0$ . Again for  $l/K = 0$  and  $4^\circ$  angle of attack, the impingement extends to the trailing edge for the NACA 65A004 airfoil.

The physical shape of the airfoil is also a predominate factor in determining the rearward limit of impingement for moderately large drops and moderately high momentum associated with values of  $l/K \approx 1$ . The trajectories for  $l/K \approx 1$  often approach the tangency point very gradually, as shown in figure 12. This very gradual approach of the lower tangent trajectory is especially true for the 4-percent-thick airfoil; and, because of it, the values of  $S_l$  are influenced appreciably by the shape of the lower surface and are also subject to personal interpretation as to the location of the tangency point. Although any change in airfoil design that alters the shape of the lower surface will change the limit of impingement for  $l/K \approx 1$ , the limit is shown in figure 13 as a function of thickness ratio because the thickness ratio is considered the principal variable defining the geometry of the airfoils. For the size drops associated with values of  $l/K \approx 1$ , the limit of impingement on the lower surface is probably not influenced appreciably by the differences in the air-flow field that result from differences in the mean camber line or the thickness ratios among the three airfoils.

The rearward limits of impingement for  $l/K = 10$  and 100 are also shown in figure 13. For large values of  $l/K$  ( $l/K \approx 100$ ) the impingement is confined to the region near the leading edge, where the shape of the airfoil is defined by the leading-edge radius (table I), which is closely related to the thickness ratio.

At an angle of attack of  $4^{\circ}$  and zero thickness ratio, the limit of impingement approaches the trailing edge, as indicated by the extrapolation in figure 13. For small values of  $1/K$  ( $1/K \approx 0$ ), the impingement is distributed nearly evenly over the bottom surface of the flat plate; however, for values of  $1/K \approx 100$  the local rates of impingement will be very small except in the neighborhood of the stagnation line. The local rates of impingement will be discussed in a subsequent section.

A much sharper limit of impingement can be anticipated for thick and blunt-nosed airfoils flying through nonuniform clouds containing large droplets than for thin airfoils. On thin airfoils, the larger droplets in the cloud will probably skim along very near the lower surface until they are stopped by small-scale perturbations caused by air-flow and surface irregularities. This skimming may result in light ice formations farther back than indicated by the limits given in figures 5, 7, and 13.

9E62

CI-2 back

#### Rate of Water Interception

Rate of total water. - The effect of thickness ratio on the rate of total water interception is summarized in figure 14. At  $4^{\circ}$  angle of attack the rate of water intercepted decreases as the thickness ratio is decreased for all flight and atmospheric conditions. The shape of the curves changes slightly as the confinement of impingement moves toward the nose of the airfoil ( $1/K \rightarrow 100$ ).

Although the rate of total water interception is determined by both the upper and lower tangent trajectories, the uncertainties in locating the lower-surface tangent point do not affect the accuracy with which the values of total water are obtained. The skimming of the droplets along the tangent trajectory near the lower surface does not introduce appreciable uncertainties in the determination of the values for  $y_{0,u} - y_{0,l}$ , from which the rate of total water interception is obtained (eq. (1)). Also, differences in the shape of the mean line among the three airfoils have a negligible influence on the total water interception as compared with the difference in thickness ratio.

Local rate of droplet impingement. - The effect of thickness ratio on the local impingement efficiency  $\beta$  is shown in figure 15. The general effect of a decrease in airfoil thickness is to shift the impingement from the upper surface to the lower surface and to spread the water more evenly over the lower surface. Also, as was discussed in the preceding section, the rate of total water interception

$$\frac{W_m}{w} = 0.33UL(y_{0,u} - y_{0,l}) = 0.33U \int_{S_l}^{S_u} \beta ds$$

decreases as the airfoil thickness is decreased; therefore, the local rates for the 4-percent-thick airfoil are generally lower than for the two thicker airfoils.

#### Summary of Comparison

The three airfoils with 12-, 8-, and 4-percent thickness were compared at the same flight and atmospheric conditions and at an angle of attack of  $4^{\circ}$ . The limit of rearward impingement on the upper surface decreases for all flight and atmospheric conditions as the airfoil thickness ratio is decreased. The rearward limit of impingement on the lower surface increases appreciably for conditions involving values of  $1/K \leq 1$  (for example,  $U \geq 400$  mph,  $d \geq 80$  microns, and  $L \leq 12.5$  ft) as the thickness ratio is decreased; but for  $1/K \geq 10$  ( $d \leq 25$  microns), the limit increases only slightly as the thickness is decreased from 12 to 4 percent. At a positive angle of attack of  $4^{\circ}$ , the rearward limit on the lower surface will increase rapidly for airfoil thickness less than 4 percent, because the impingement extends to the trailing edge on a flat plate of zero thickness ratio. The total water intercepted, however, decreases as the airfoil thickness decreases; therefore, in general, a decrease in thickness ratio will result in less total water being spread over a larger area of the lower surface.

#### CONCLUDING REMARKS

The data presented herein apply directly to flights in clouds composed of droplets that are all uniform in size and to nonswept wings of high aspect ratio. A detailed procedure for weighting the impingement of droplets for flights in nonuniform clouds is presented in reference 2. A method for extending the impingement calculations for nonswept wings to swept wings is presented in reference 7. The data presented in this report for the NACA 65A004 airfoil also apply to wings with some taper, provided that for each section of span considered the taper is small enough to permit the approximation of two-dimensional flow over the section.

As previously stated, equations and graphical procedure for translating the dimensionless parameters used in this report into terms of airplane speed, chord length, altitude, and droplet size are presented in appendix B of reference 1.

Lewis Flight Propulsion Laboratory  
National Advisory Committee for Aeronautics  
Cleveland, Ohio, September 17, 1953

## REFERENCES

- 9268
1. Brun, Rinaldo J., Gallagher, Helen M., and Vogt, Dorothea E.: Impingement of Water Droplets on NACA 65<sub>1</sub>-208 and 65<sub>1</sub>-212 Airfoils at 4° Angle of Attack. NACA TN 2952, 1953.
  2. Brun, Rinaldo J., and Mergler, Harry W.: Impingement of Water Droplets on a Cylinder in an Incompressible Flow Field and Evaluation of Rotating Multicylinder Method for Measurement of Droplet-Size Distribution, Volume-Medium Droplet-Size, and Liquid-Water Content in Clouds. NACA TN 2904, 1953.
  3. Theodorsen, T., and Garrick, I. E.: General Potential Theory of Arbitrary Wing Sections. NACA Rep. 452, 1933.
  4. Brun, Rinaldo J., Serafini, John S., and Gallagher, Helen M.: Impingement of Cloud Droplets on Aerodynamic Bodies as Affected by Compressibility of Air Flow Around the Body. NACA TN 2903, 1953.
  5. Guibert, A. G., Janssen, E., and Robbins, W. M.: Determination of Rate, Area, and Distribution of Impingement of Waterdrops on Various Airfoils from Trajectories Obtained on the Differential Analyzer. NACA RM 9A05, 1949.
  6. Abbott, Ira H., and von Doenhoff, Albert E.: Theory of Wing Sections. First ed., McGraw-Hill Book Co., Inc., 1949.
  7. Dorsch, Robert G., and Brun, Rinaldo J.: A Method for Determining Cloud-Droplet Impingement on Swept Wings. NACA TN 2931, 1953.

TABLE I. - AIRFOIL COORDINATE POINTS

(a) 65A004 Airfoil; leading-edge radius, 0.00102.

Symmetrical			Symmetrical		
x'	y'	S	x'	y'	S
0	0	0	0.3500	0.01967	0.35189
.00025	.0007	.00080	.4000	.02000	.40189
.00050	.00098	.00118	.4500	.01998	.45189
.00100	.00140	.00183	.5000	.01957	.50189
.0025	.00226	.00356	.5500	.01875	.55190
.0050	.00314	.00621	.6000	.01754	.60191
.0075	.00381	.00880	.6500	.01597	.65193
.0100	.00437	.01136	.7000	.01410	.70197
.0125	.00485	.01391	.7500	.01200	.75201
.0175	.00566	.01898	.8000	.00972	.80206
.0250	.00659	.02654	.8500	.00735	.85212
.0375	.00777	.03910	.9000	.00494	.90218
.0500	.00879	.05164	.9500	.00250	.95224
.0750	.01061	.07671	.9600	.00200	.96225
.1000	.01215	.10176	.9700	.00150	.97226
.1500	.01464	.15182	.9800	.00100	.98227
.2000	.01655	.20186	.9900	.00050	.99228
.2500	.01798	.25188	1.0000	0	1.00229
.3000	.01900	.30189			

TABLE I. - Continued. AIRFOIL COORDINATE POINTS

(b) 65<sub>1</sub>-208 Airfoil; leading-edge radius, 0.00434; slope through leading edge, 0.084.

Upper surface			Lower surface		
x'	y'	s	x'	y'	s
0	0	0	0	0	0
.00447	.00675	.00820	.00553	.00575	.00798
.00691	.00824	.01106	.00809	.00684	.01076
.01184	.01050	.01648	.01316	.00836	.01605
.02426	.01451	.02953	.02574	.01079	.02886
.04918	.02060	.05518	.05082	.01428	.05418
.07415	.02540	.08061	.07585	.01692	.07935
.09915	.02948	.10594	.10085	.01914	.10445
.14919	.03603	.15641	.15081	.02257	.15453
.19927	.04107	.20674	.20073	.02515	.20452
.24937	.04493	.25699	.25063	.02703	.25446
.29949	.04777	.30719	.30051	.02833	.30436
.34961	.04968	.35735	.35039	.02908	.35425
.39974	.05069	.40749	.40026	.02927	.40412
.44987	.05069	.45762	.45013	.02879	.45399
.50000	.04960	.50776	.50000	.02754	.50414
.55012	.04733	.55793	.54988	.02543	.55407
.60022	.04408	.60814	.59978	.02266	.60405
.65029	.04001	.65838	.64971	.01941	.65409
.70034	.03525	.70866	.69960	.01581	.70417
.75037	.02991	.75897	.74963	.01201	.75428
.80036	.02413	.80929	.79964	.00821	.80443
.85031	.01804	.85961	.84969	.00458	.85461
.90023	.01181	.90992	.89977	.00147	.90479
.95012	.00568	.96018	.94988	.00064	.95494
1.00000	0	1.01038	1.00000	0	1.00506

TABLE I. - Concluded. AIRFOIL COORDINATE POINTS

(c) 65<sub>1</sub>-212 Airfoil; leading-edge radius, 0.01000; slope through leading edge, 0.096.

Upper surface			Lower surface		
x'	y'	S	x'	y'	S
0	0	0	0	0	0
.00423	.00970	.0100	.00577	.00870	.01
.00664	.01176	.0135	.00836	.01036	.014
.01154	.01491	.0190	.01346	.01277	.019
.02391	.02058	.0325	.02609	.01686	.0325
.04878	.02919	.0580	.05122	.02287	.0580
.07373	.03593	.0840	.07627	.02745	.0830
.09873	.04162	.1095	.10127	.03128	.1090
.14879	.05073	.1610	.15121	.03727	.1600
.19890	.05770	.2120	.20110	.04178	.2090
.24906	.06300	.2620	.25094	.04510	.2590
.29923	.06687	.3125	.30077	.04743	.3090
.34942	.06942	.3630	.35058	.04882	.3590
.39961	.07068	.4135	.40039	.04926	.4090
.44981	.07044	.4640	.45019	.04854	.4605
.50000	.06860	.5150	.50000	.04654	.5110
.55017	.06507	.5705	.54983	.04317	.5610
.60032	.06014	.6210	.59968	.03872	.6115
.65043	.05411	.6720	.64957	.03351	.6625
.70050	.04715	.7230	.69950	.02771	.7125
.75053	.03954	.7730	.74947	.02164	.7640
.80052	.03140	.8240	.79948	.01548	.8135
.85045	.02302	.8750	.84955	.00956	.8640
.90033	.01463	.9265	.89967	.00429	.9140
.95017	.00671	.9775	.94983	.00039	.9650
1.00000	0	1.0275	1.00000	0	1.0150

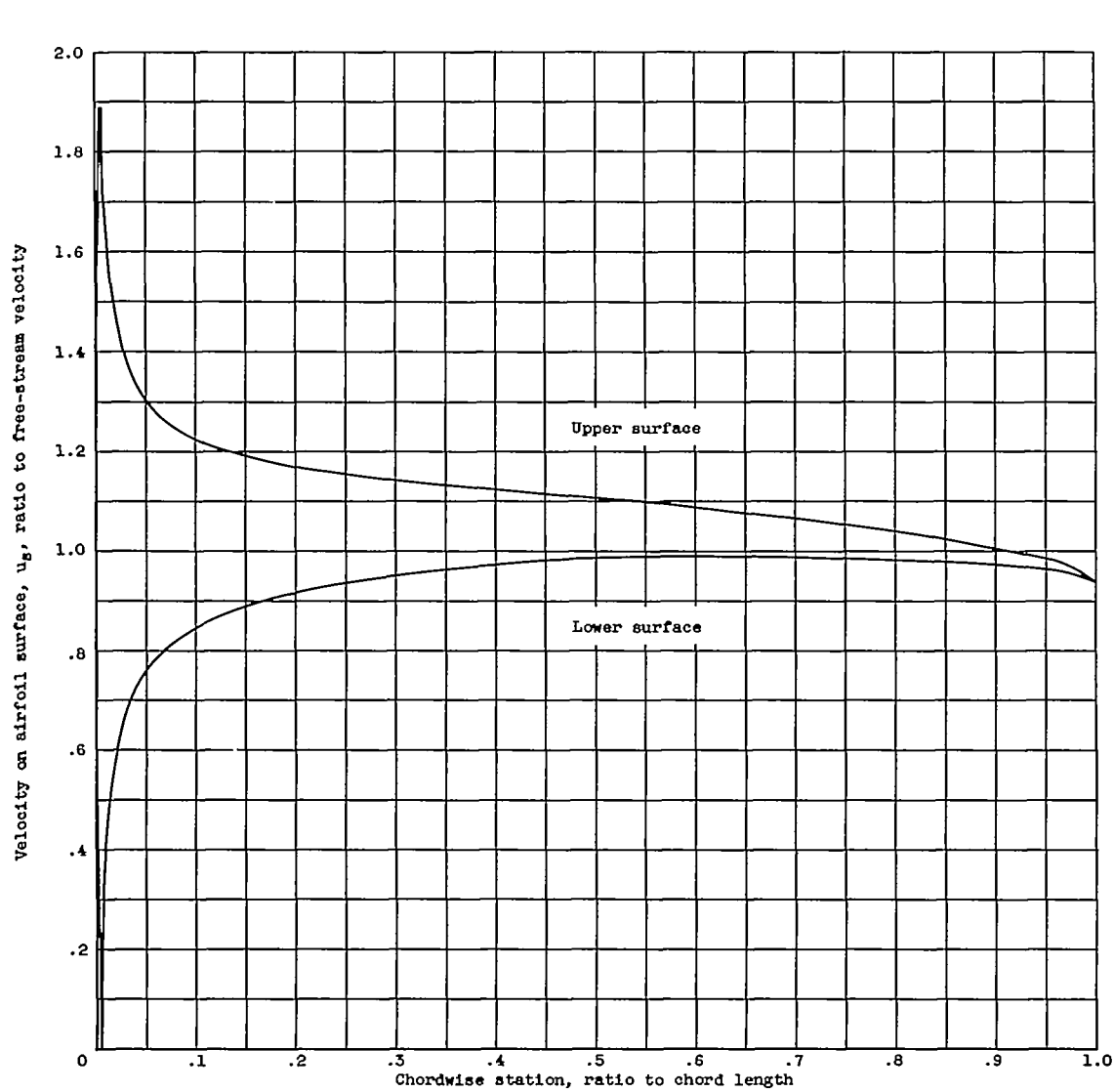


Figure 1. - Velocities on surface of 65A004 airfoil. Angle of attack,  $4^\circ$ ; incompressible flow field.

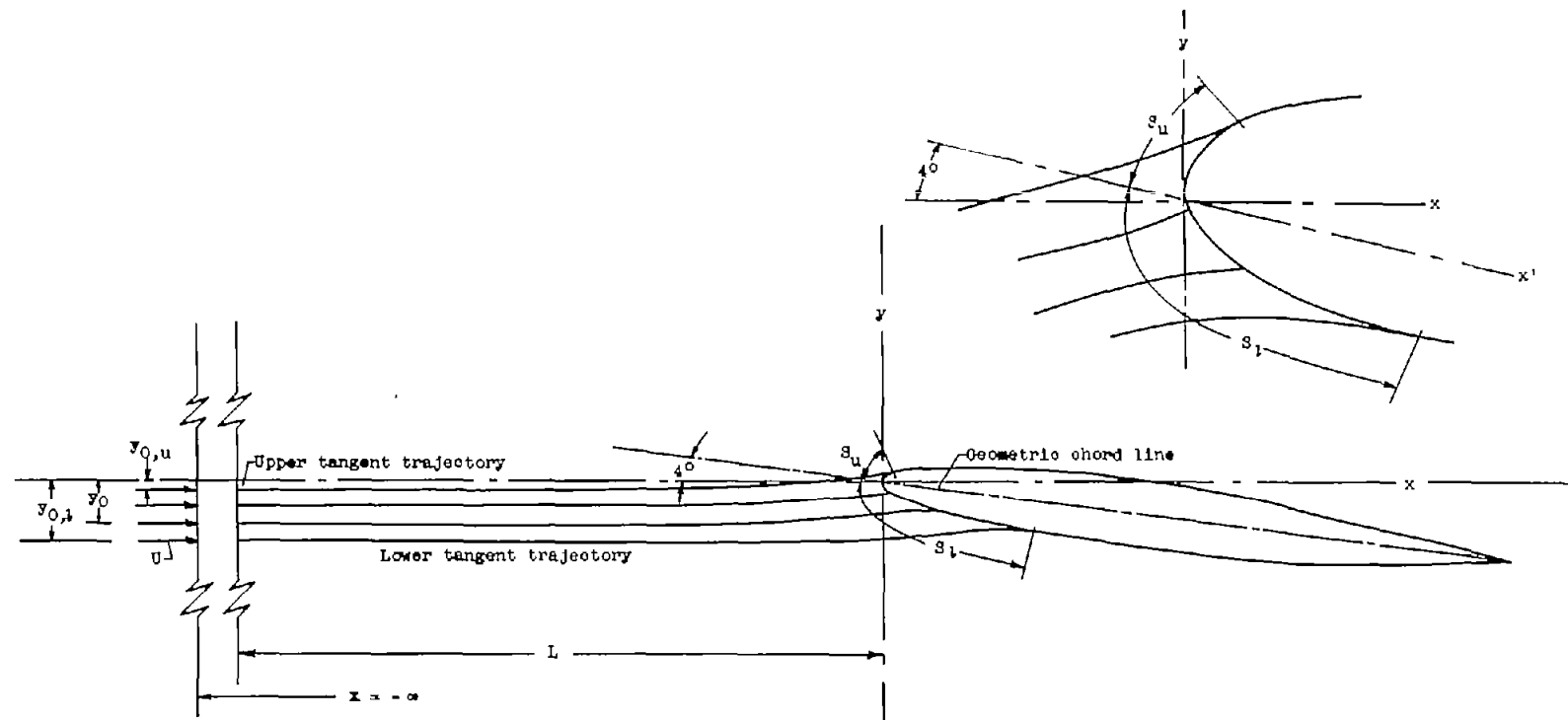
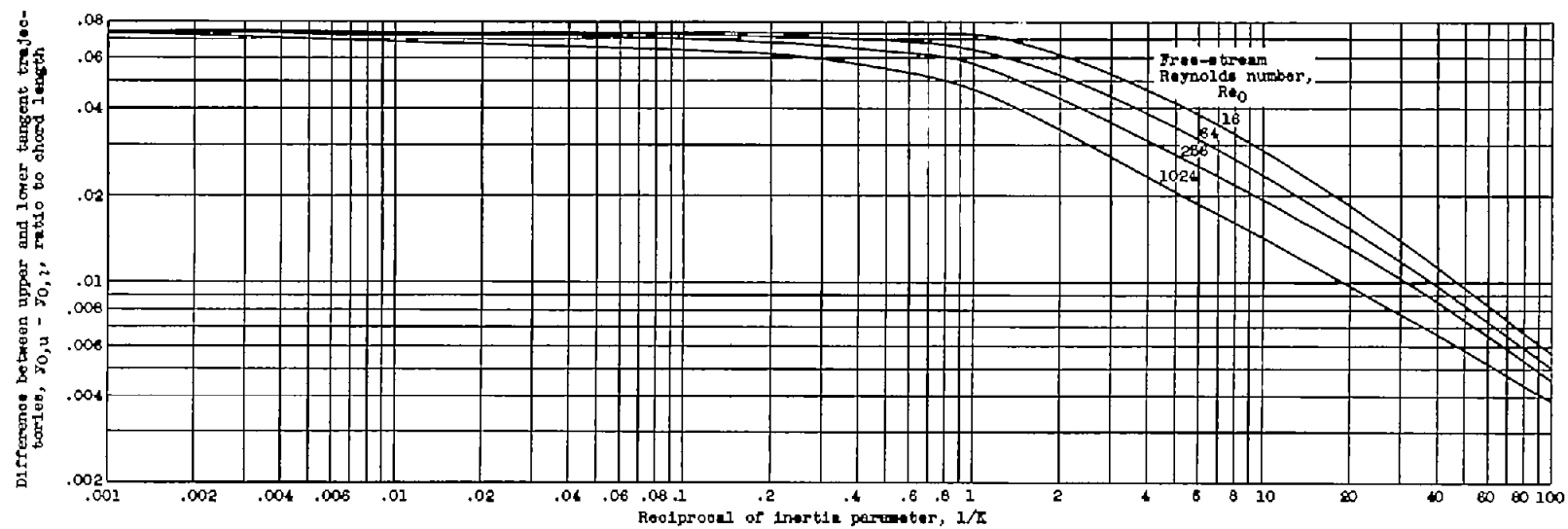
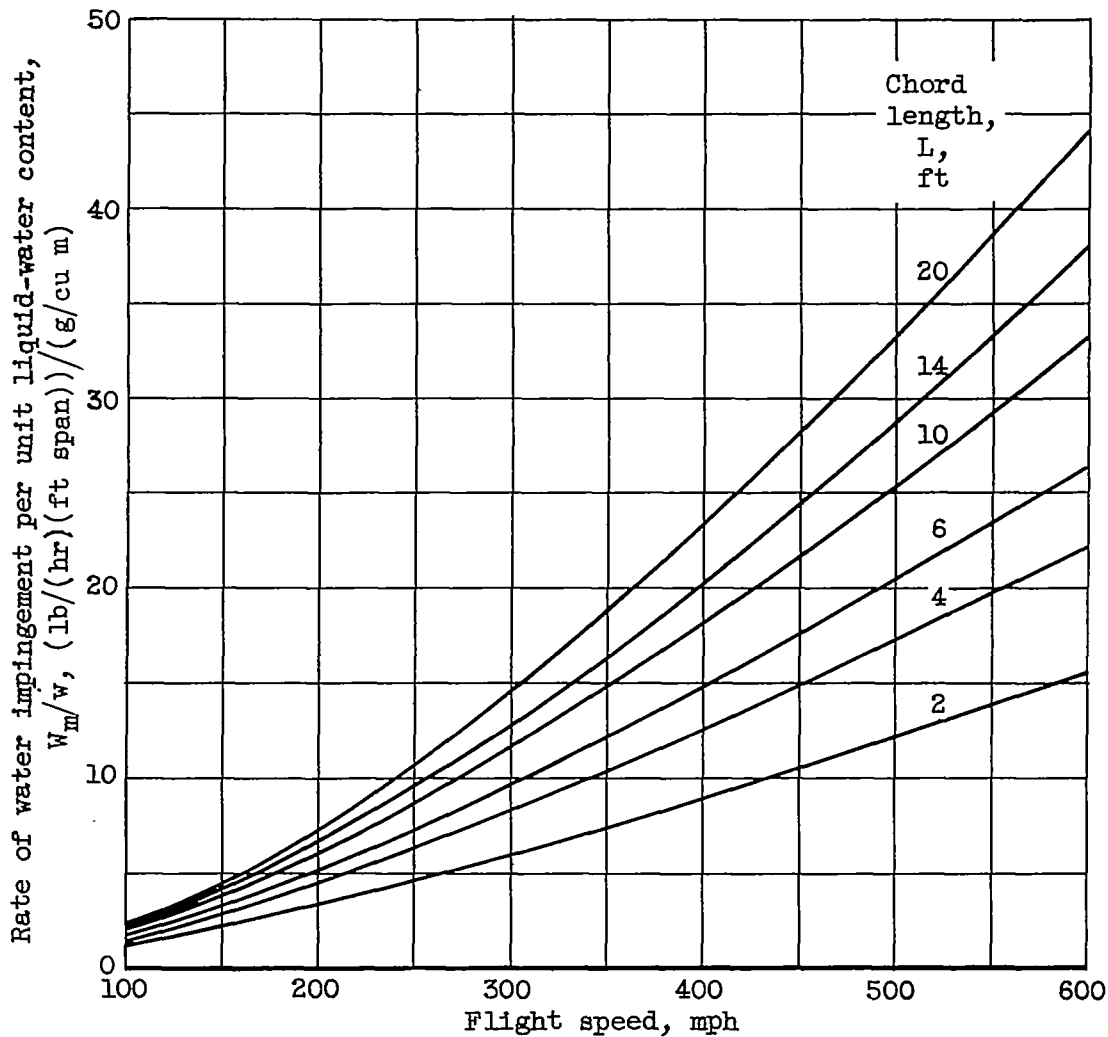


Figure 2. - Droplet trajectories with respect to airfoil.

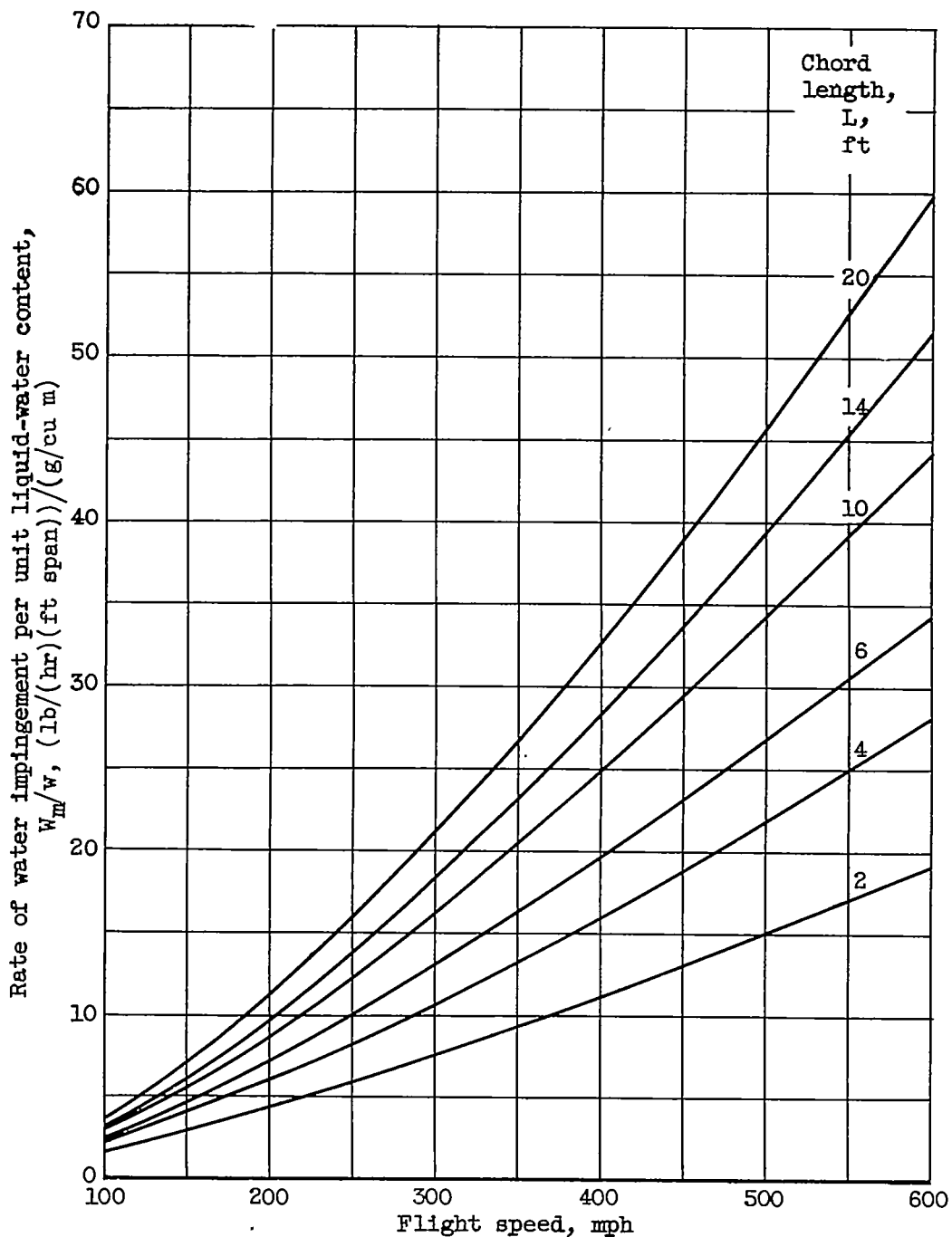




(a) Droplet size, 15 microns.

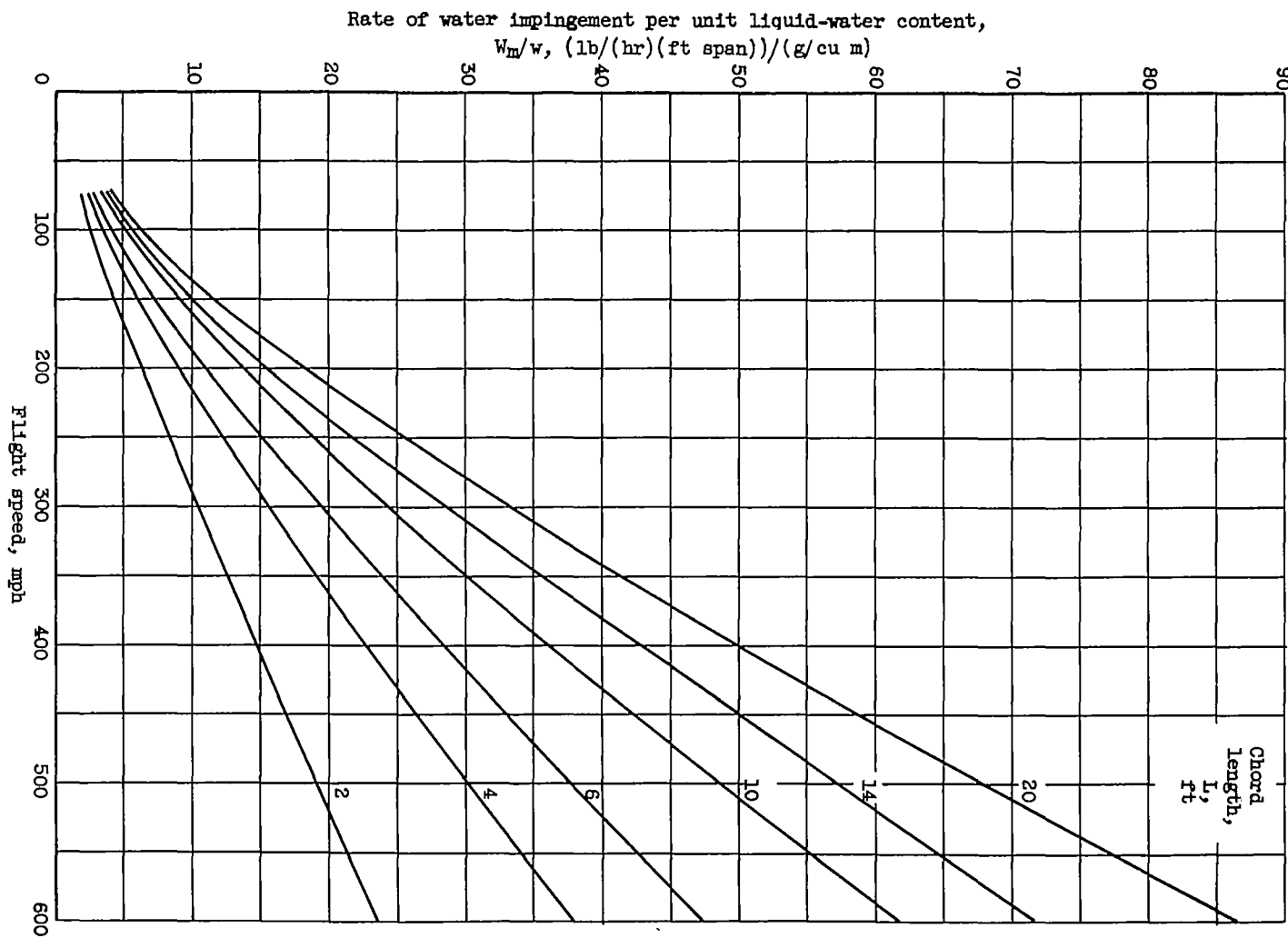
Figure 4. - Rate of water impingement on 65A004 airfoil. Angle of attack,  $4^\circ$ ; altitude, 20,000 feet; most probable icing temperature,  $-11^\circ F$ .

2936



(b) Droplet size, 20 microns.

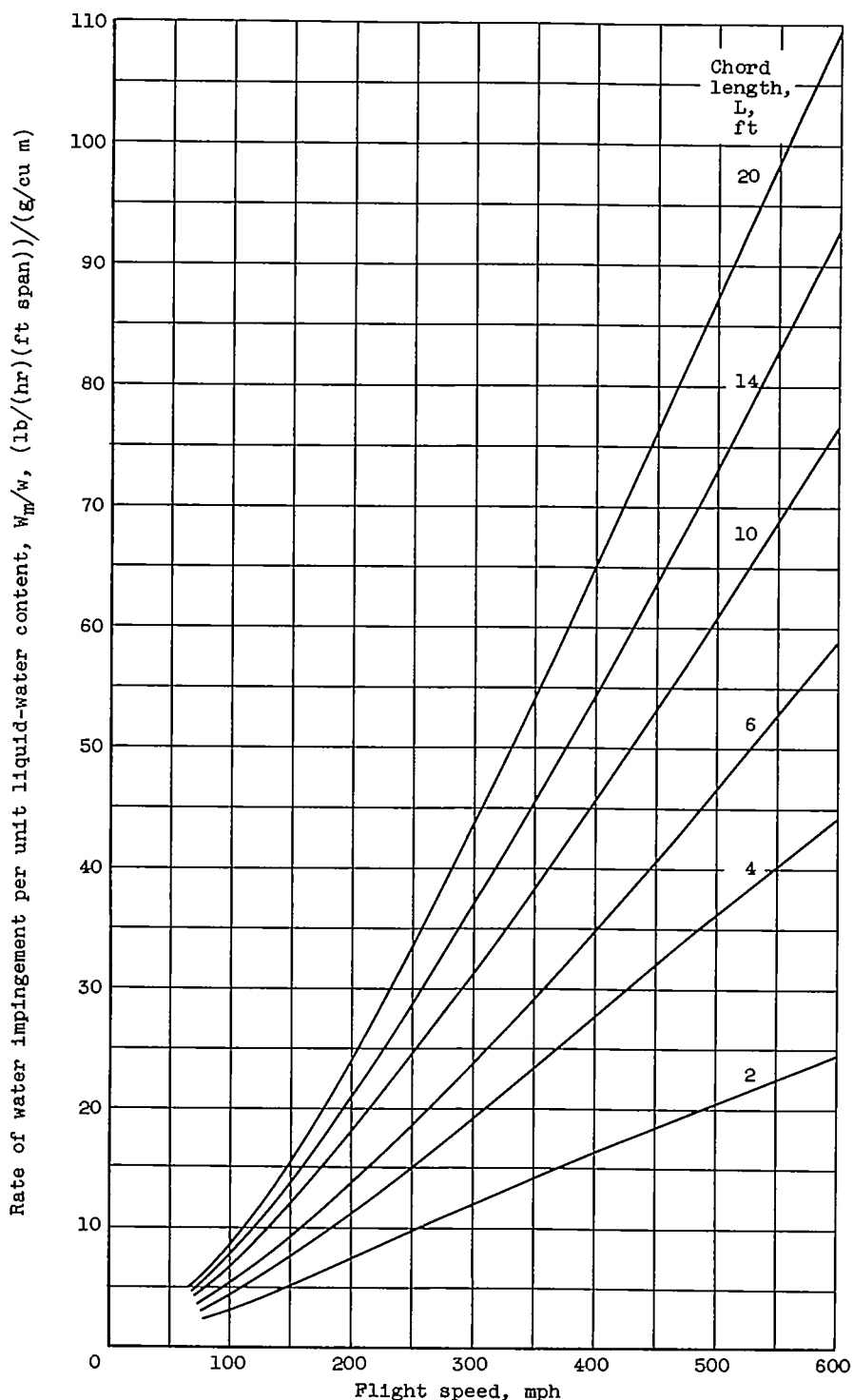
Figure 4. - Continued. Rate of water impingement on 65A004 airfoil. Angle of attack,  $4^\circ$ ; altitude, 20,000 feet; most probable icing temperature,  $-11^\circ$  F.



(c) Droplet size, 30 microns.

Figure 4. - Continued. Rate of water impingement on 65A004 airfoil. Angle of attack, 40°; altitude, 20,000 feet; most probable icing temperature, -110°F.

2936



(d) Droplet size, 40 microns.

Figure 4. - Concluded. Rate of water impingement on 65A004 airfoil. Angle of attack,  $4^\circ$ ; altitude, 20,000 feet; most probable icing temperature,  $-11^\circ \text{F}$ .

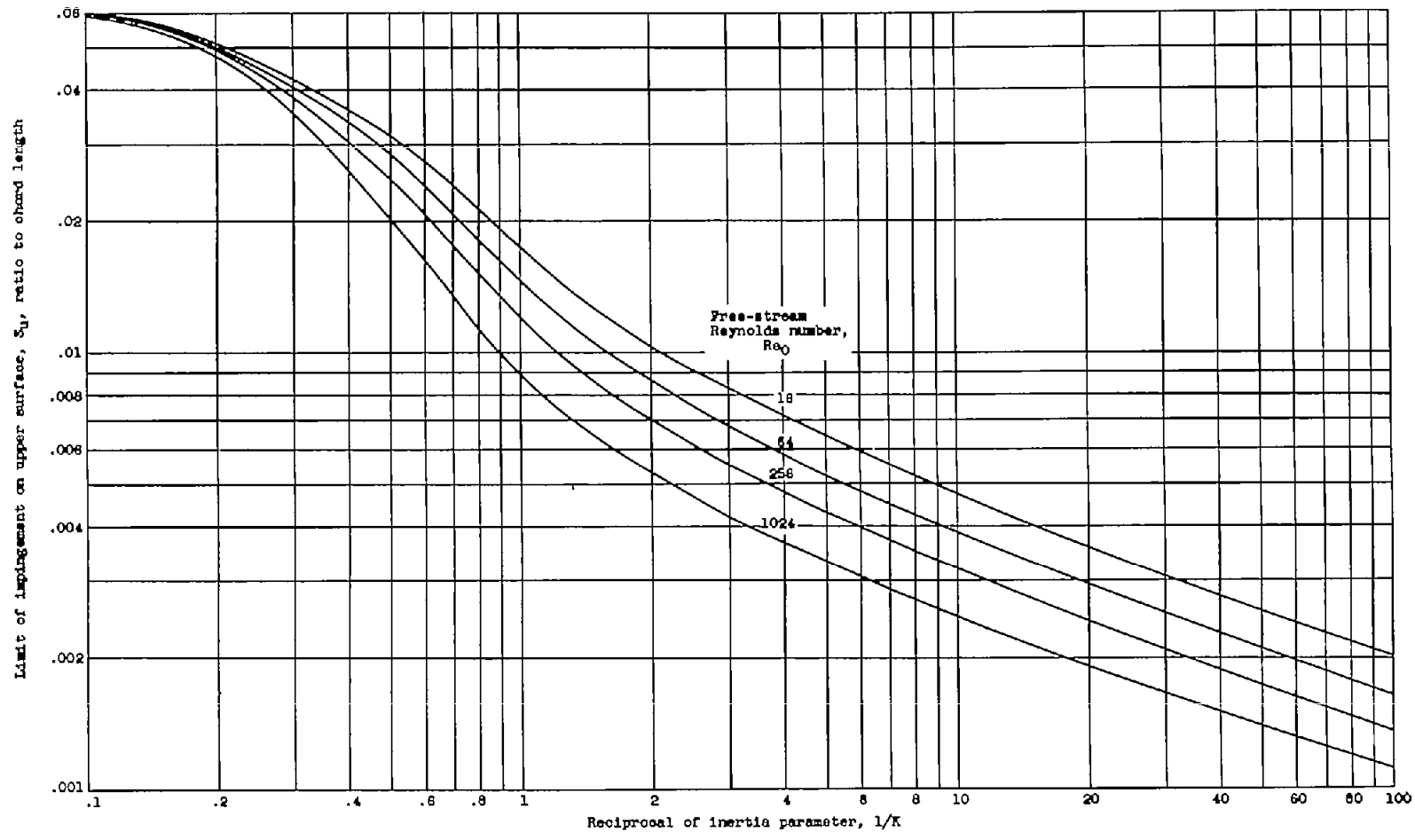


Figure 5. - Limit of impingement on surface of 65A004 airfoil. Angle of attack,  $4^\circ$ .

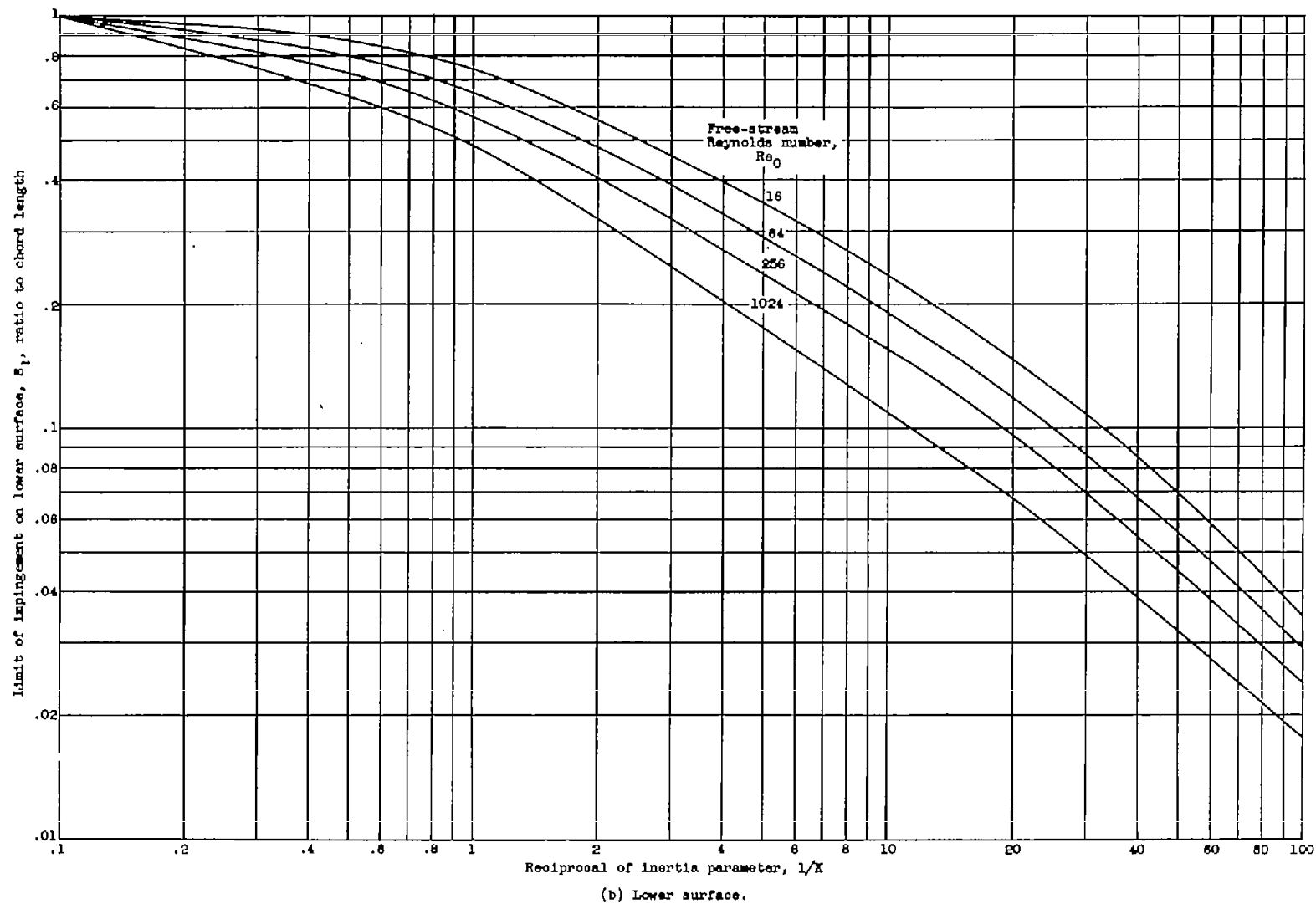
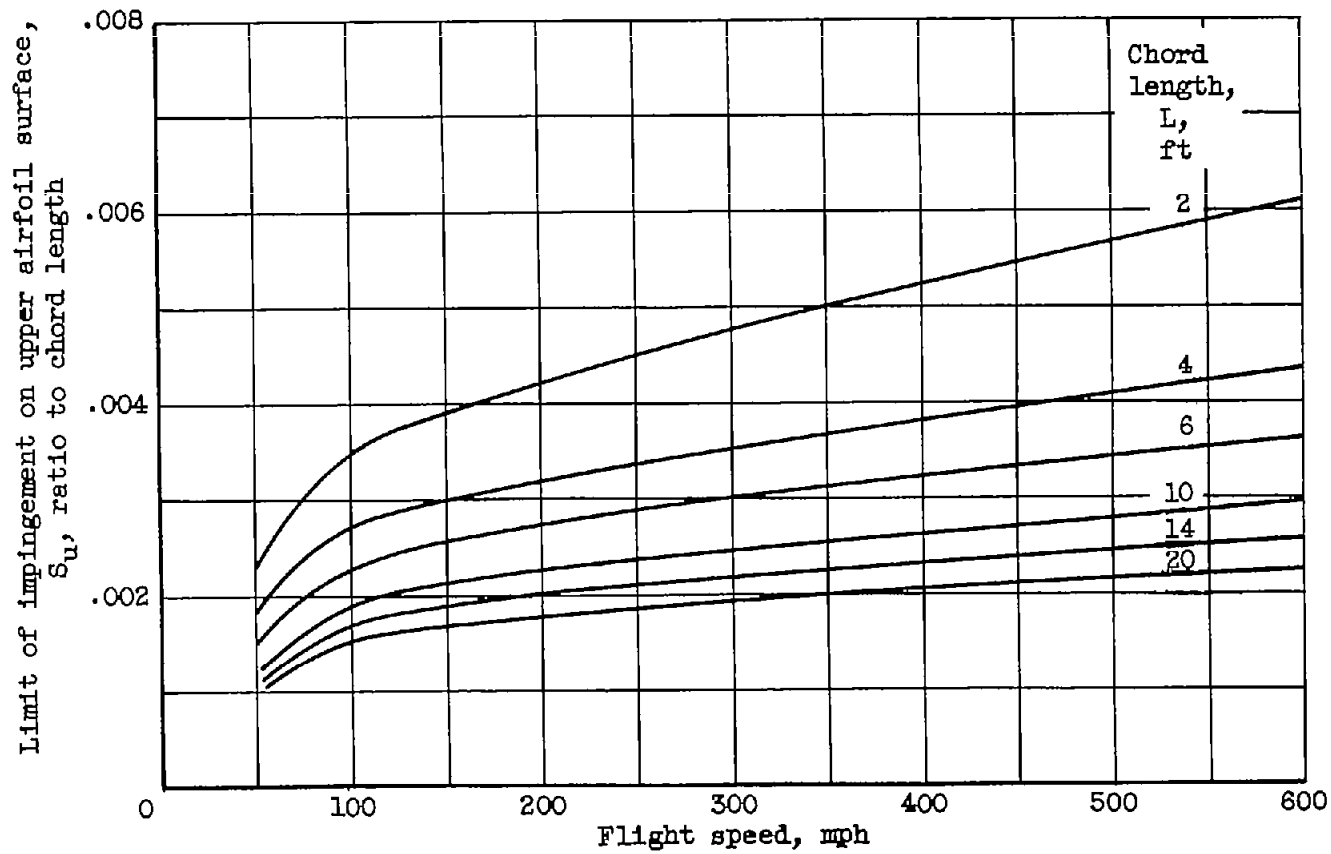
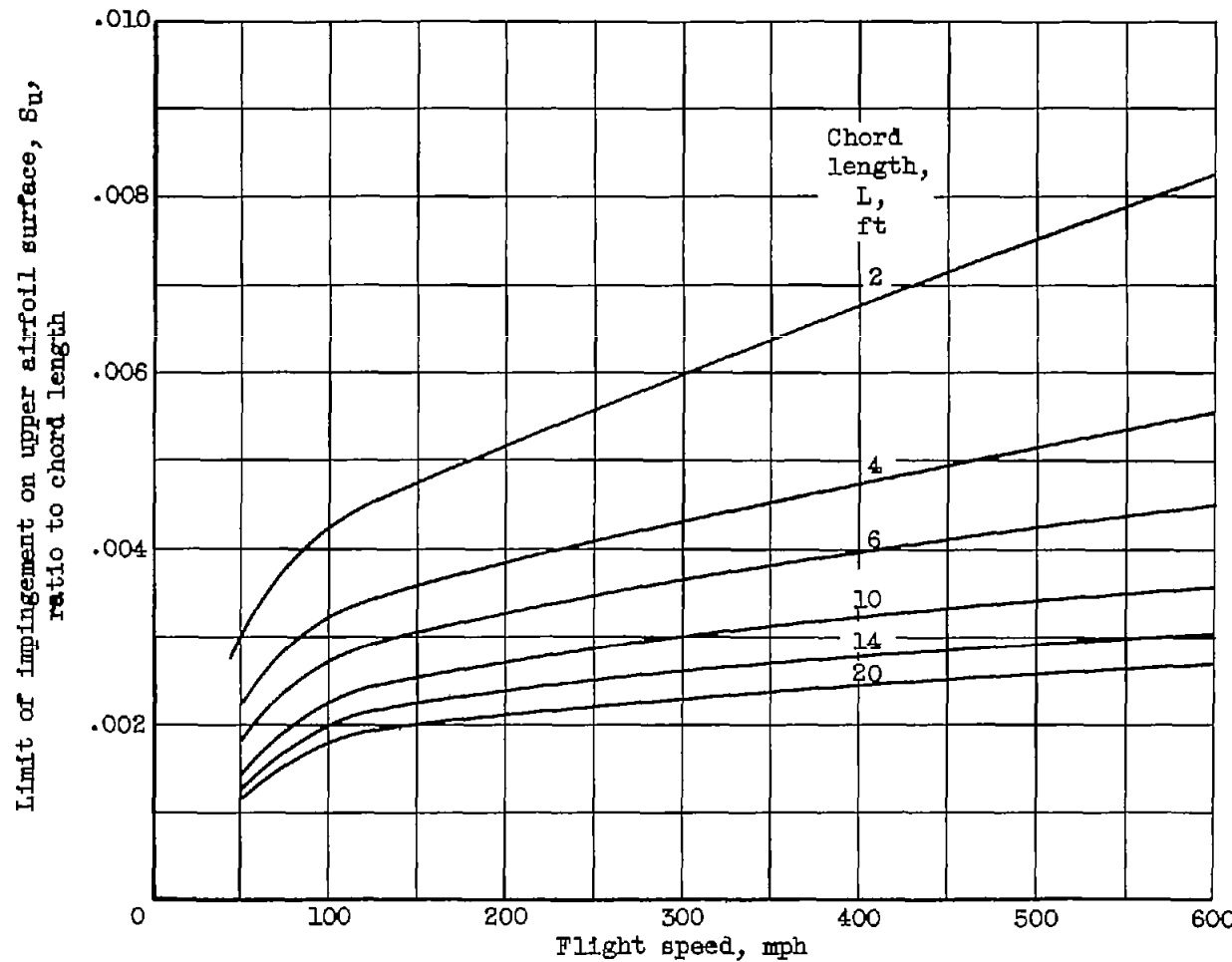


Figure 5. - Concluded. Limit of impingement on surface of 65A004 airfoil. Angle of attack,  $4^\circ$ .



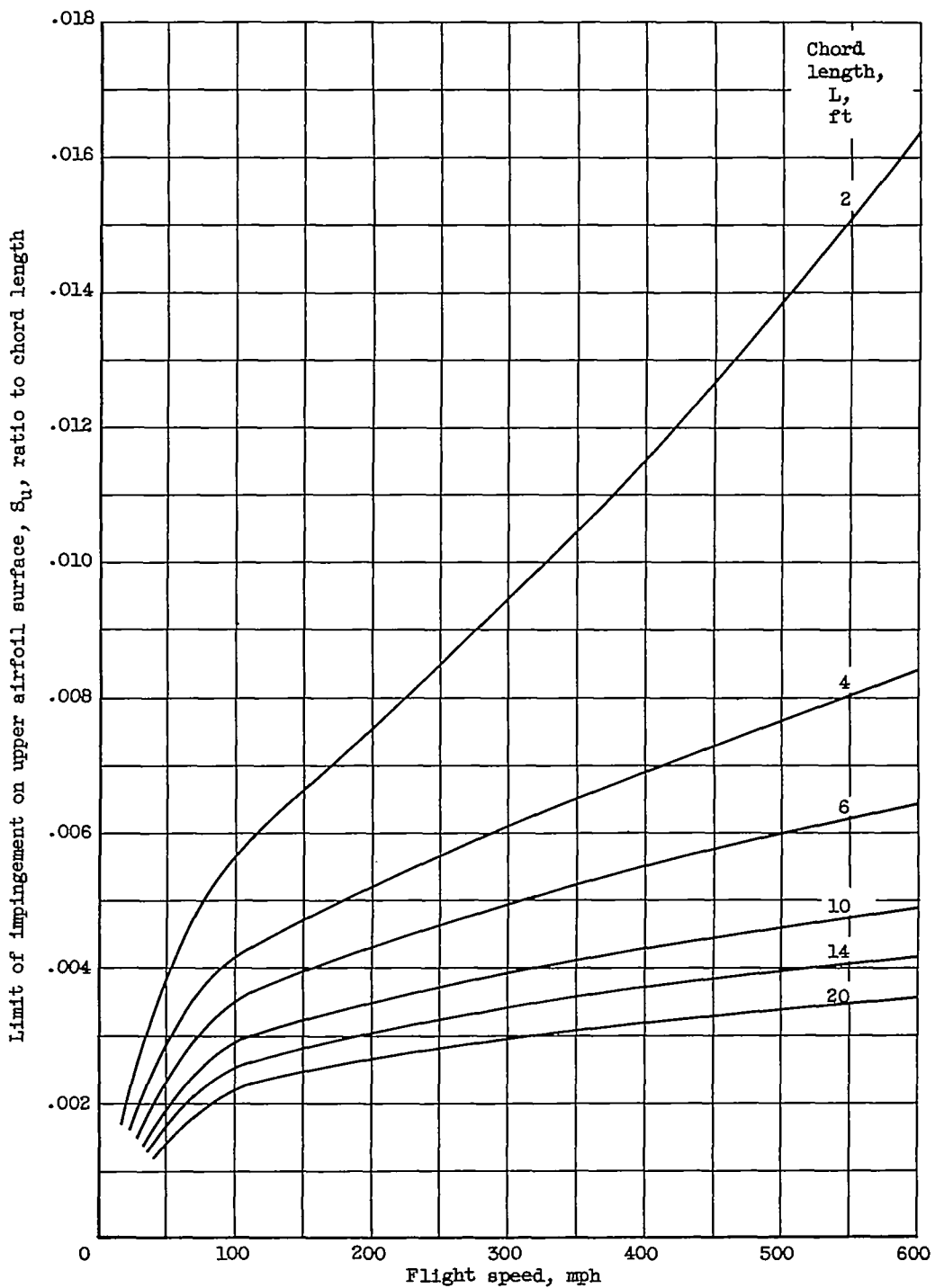
(a) Droplet size, 15 microns.

Figure 6. - Limit of impingement along upper surface of 65A004 airfoil.  
Altitude, 20,000 feet; angle of attack,  $4^\circ$ ; most probable icing temperature,  $-11^\circ F$ .



(b) Droplet size, 20 microns.

Figure 6. - Continued. Limit of impingement along upper surface of 65A004 airfoil. Altitude, 20,000 feet; angle of attack, 4°; most probable icing temperature, -11° F.



(c) Droplet size, 30 microns.

Figure 6. - Continued. Limit of impingement along upper surface of 65A004 airfoil. Altitude, 20,000 feet; angle of attack,  $4^\circ$ ; most probable icing temperature,  $-11^\circ$  F.

2936

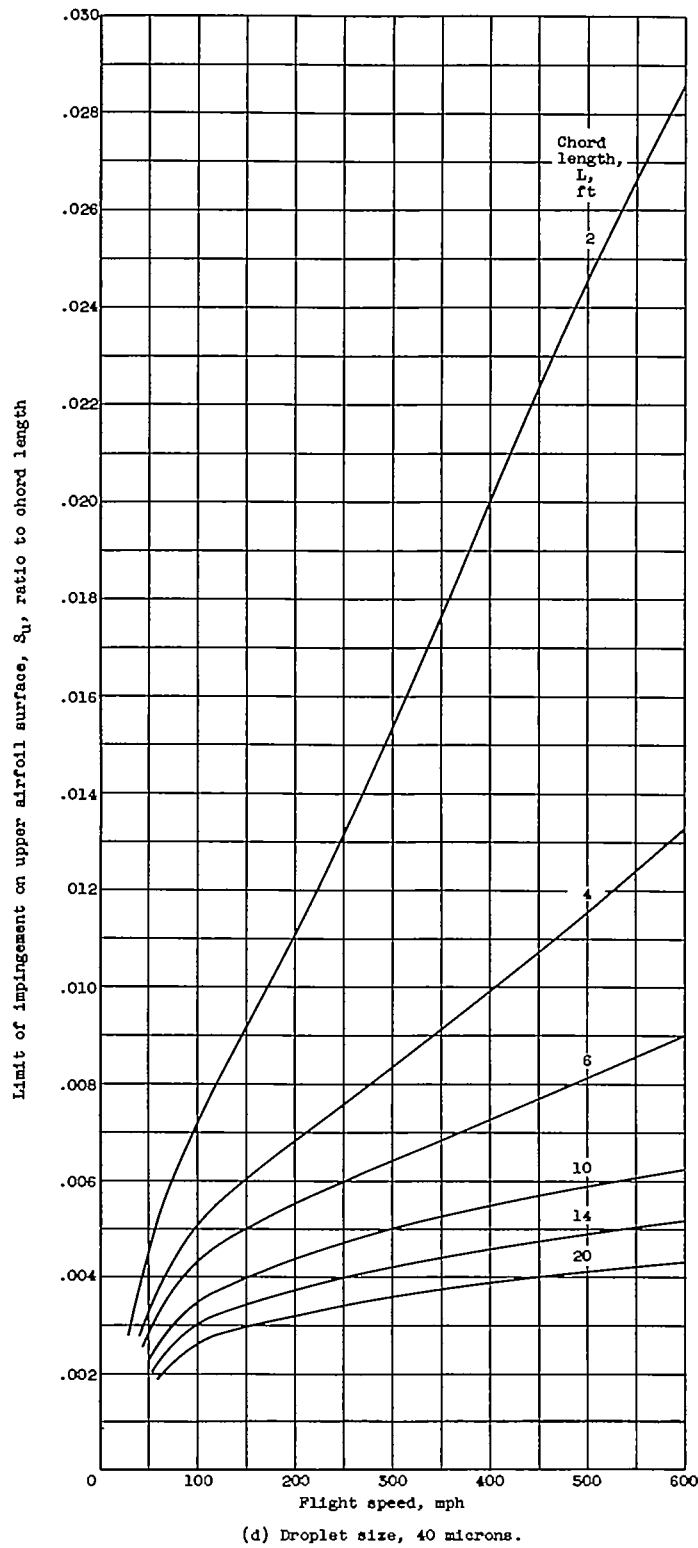
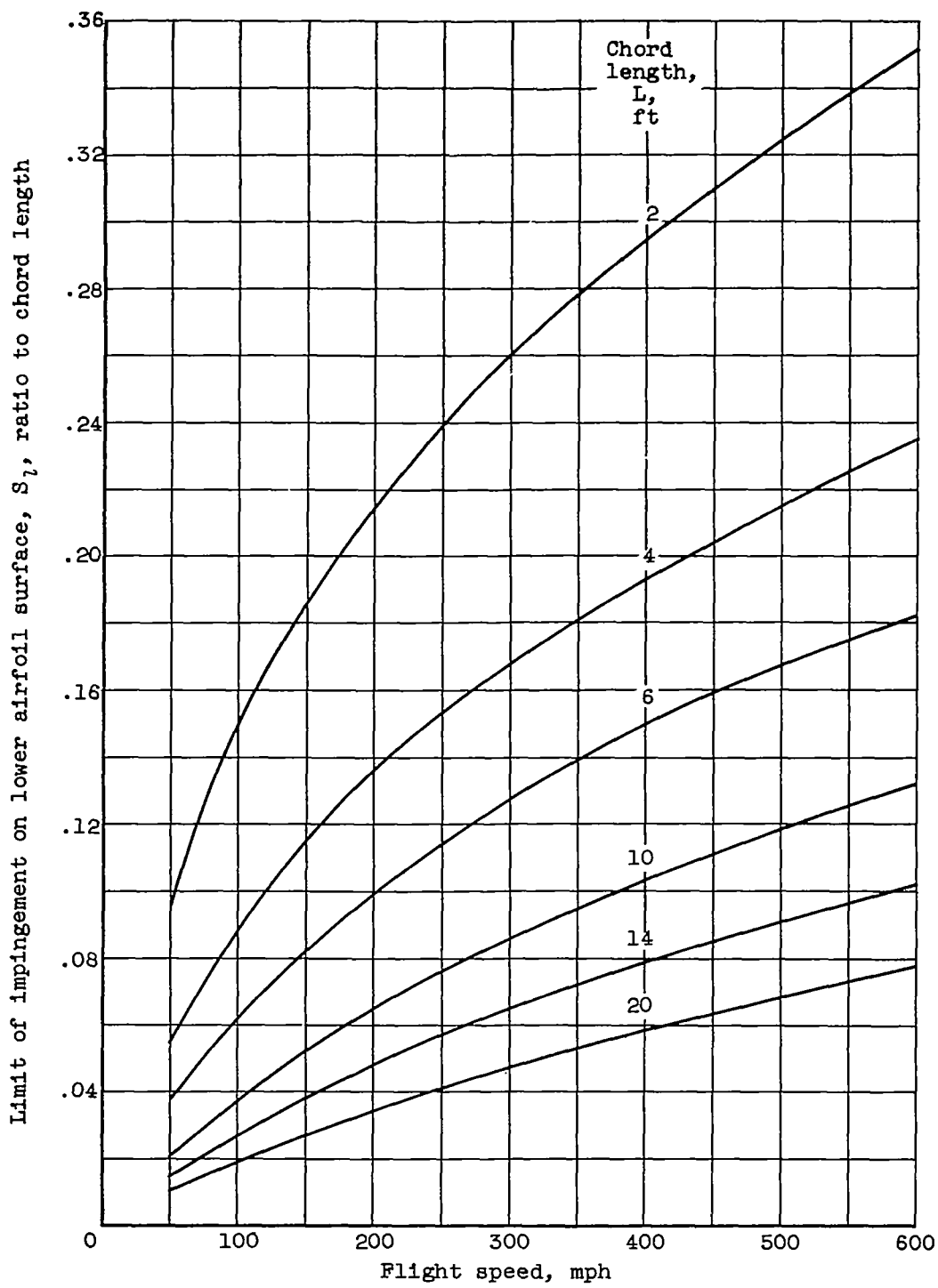
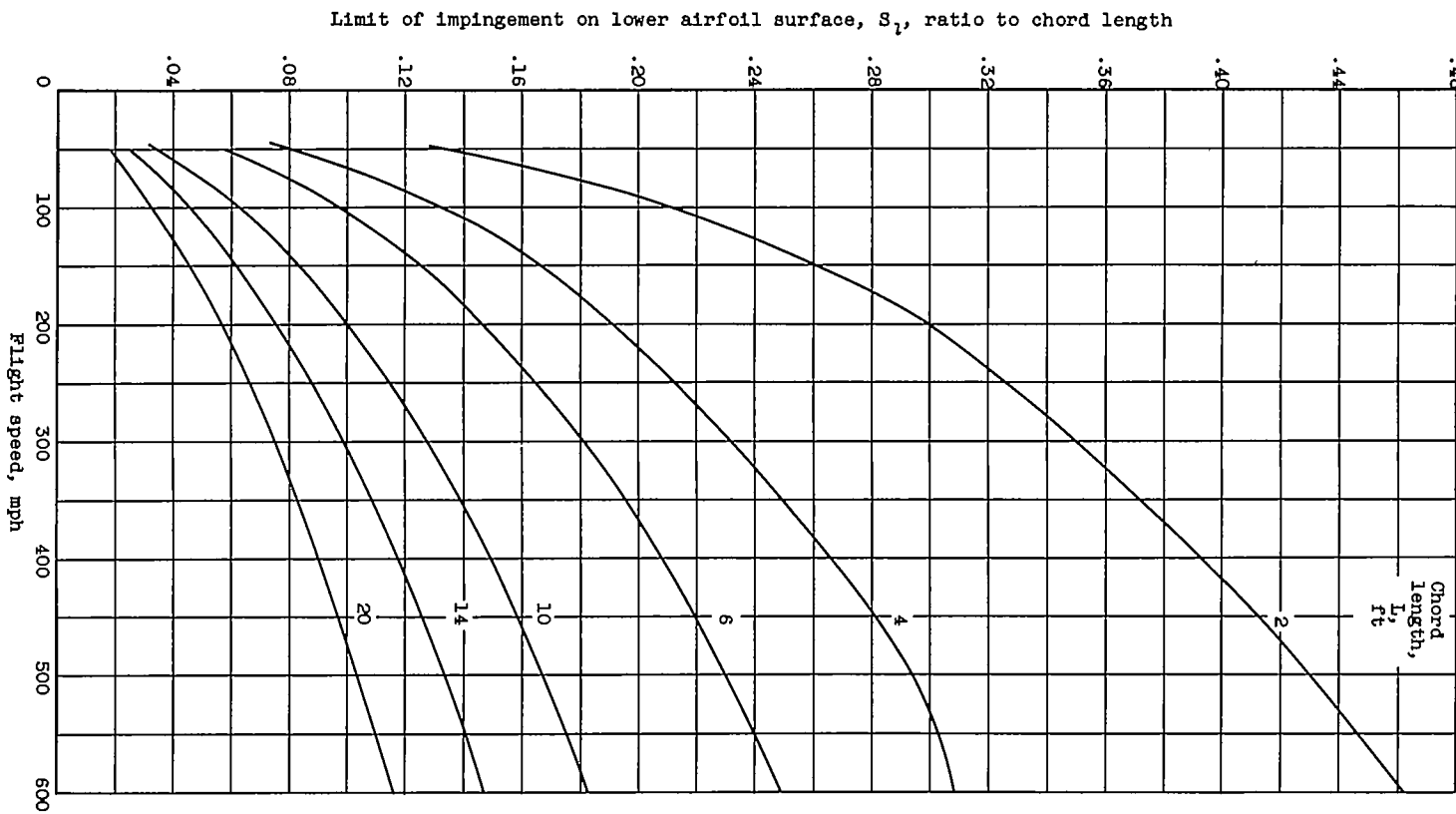


Figure 6. — Concluded. Limit of impingement along upper surface of 65A004 airfoil. Altitude, 20,000 feet; angle of attack,  $4^\circ$ ; most probable icing temperature,  $-11^\circ F$ .



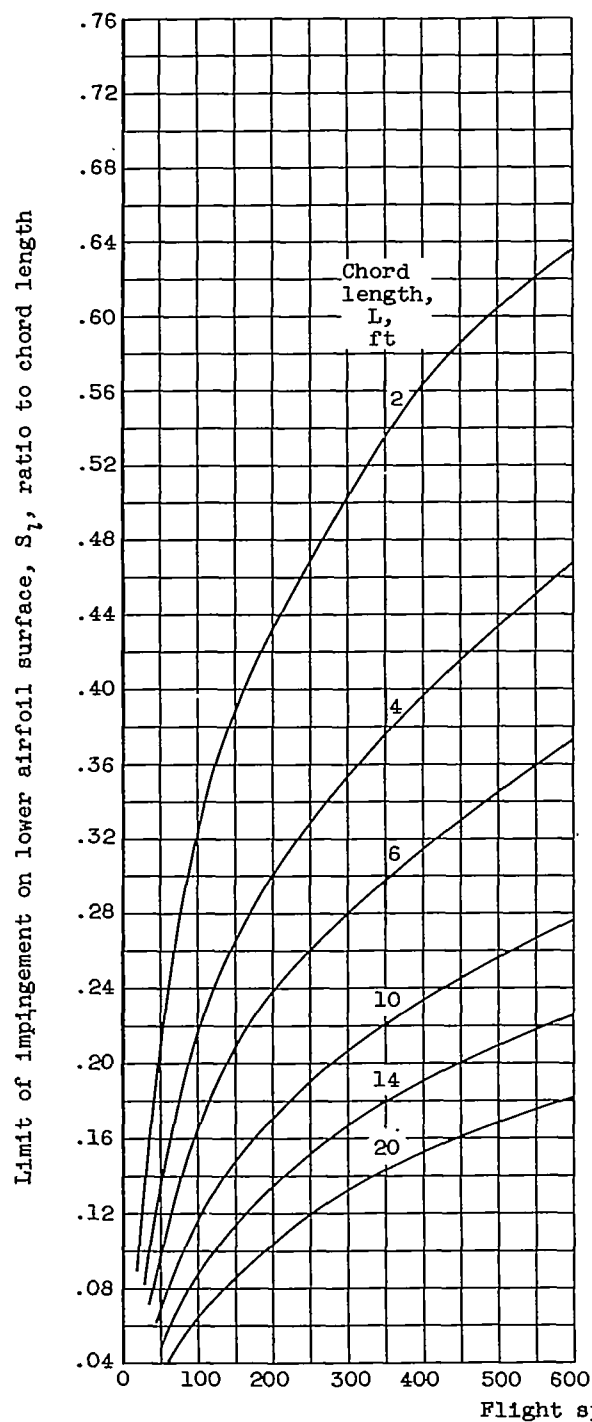
(a) Droplet size, 15 microns.

Figure 7. - Limit of impingement along lower surface of 65A004 airfoil. Altitude, 20,000 feet; angle of attack,  $4^\circ$ ; most probable icing temperature,  $-11^\circ$  F.

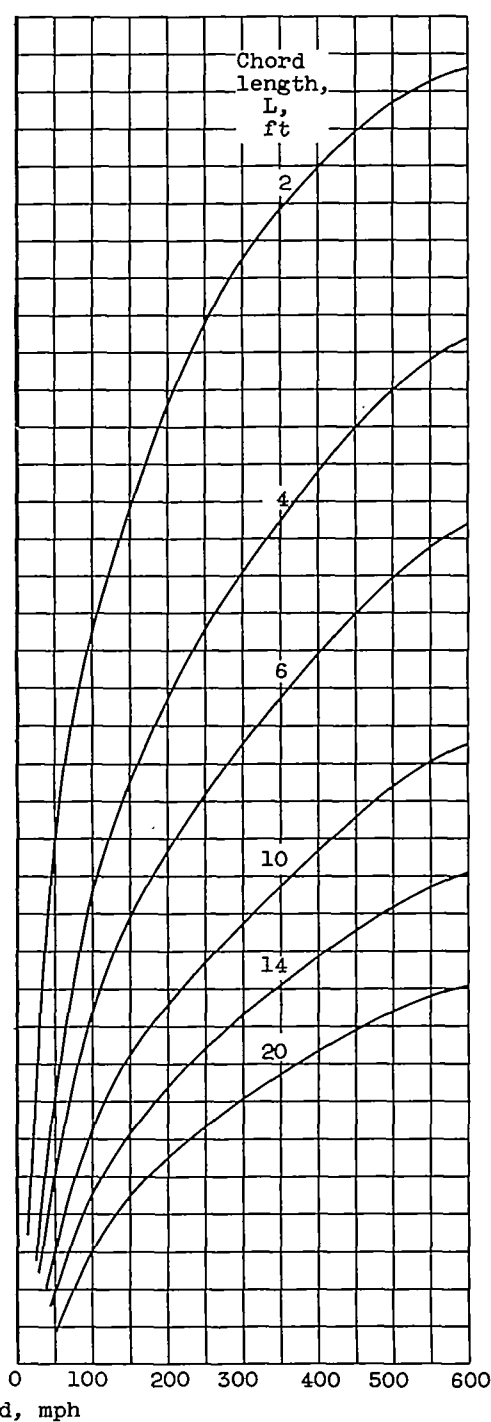


(b) Droplet size, 20 microns.

Figure 7. - Continued. Limit of impingement along lower surface of 6SA004 airfoil. Altitude, 20,000 feet; angle of attack, 40°; most probable icing temperature, -110°F.

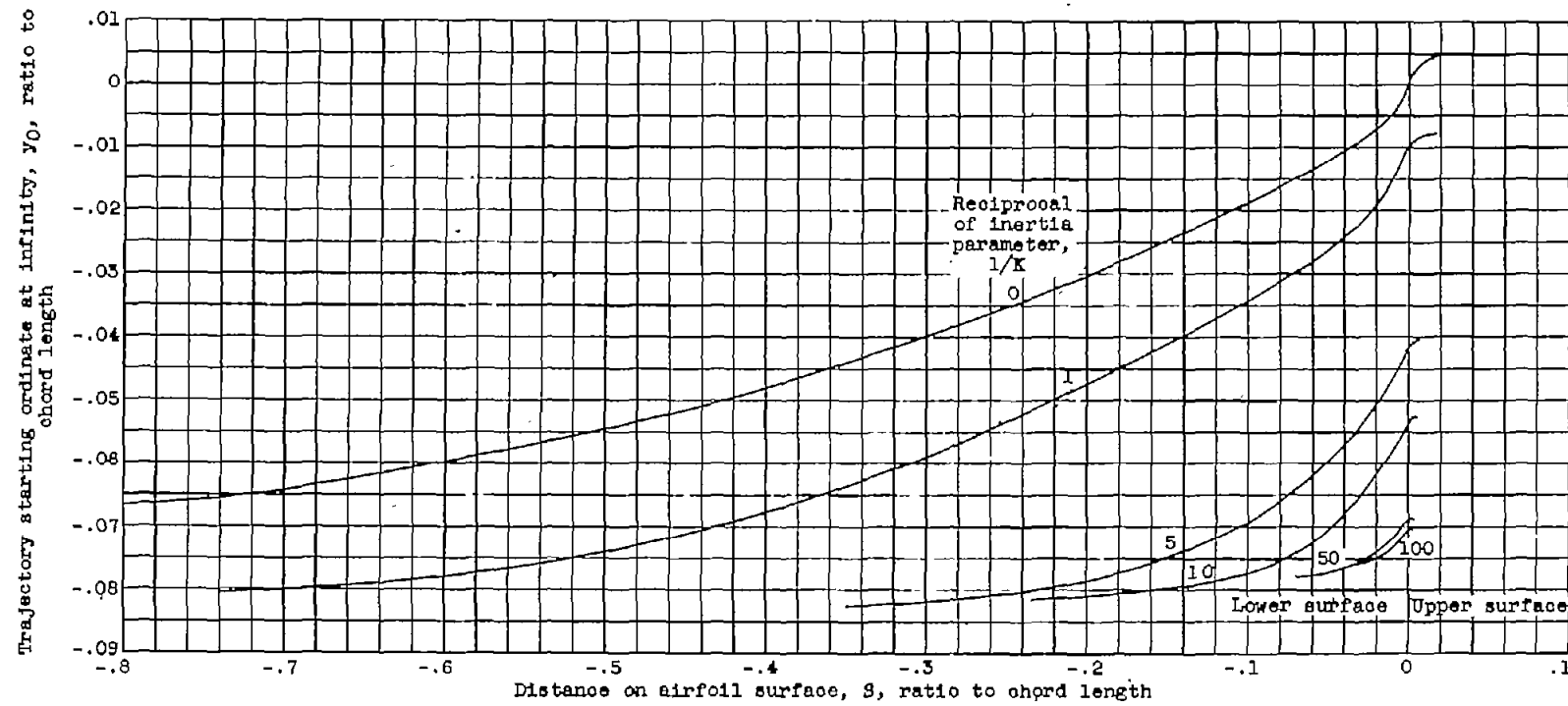


(c) Droplet size, 30 microns.



(d) Droplet size, 40 microns.

Figure 7. - Concluded. Limit of impingement along lower surface of 65A004 airfoil. Altitude, 20,000 feet; angle of attack,  $4^\circ$ ; most probable icing temperature,  $-11^\circ$  F.



(a) Free-stream Reynolds number, 16.

Figure 8. - Trajectory starting ordinates as function of point of impingement on surface of 65A004 airfoil.

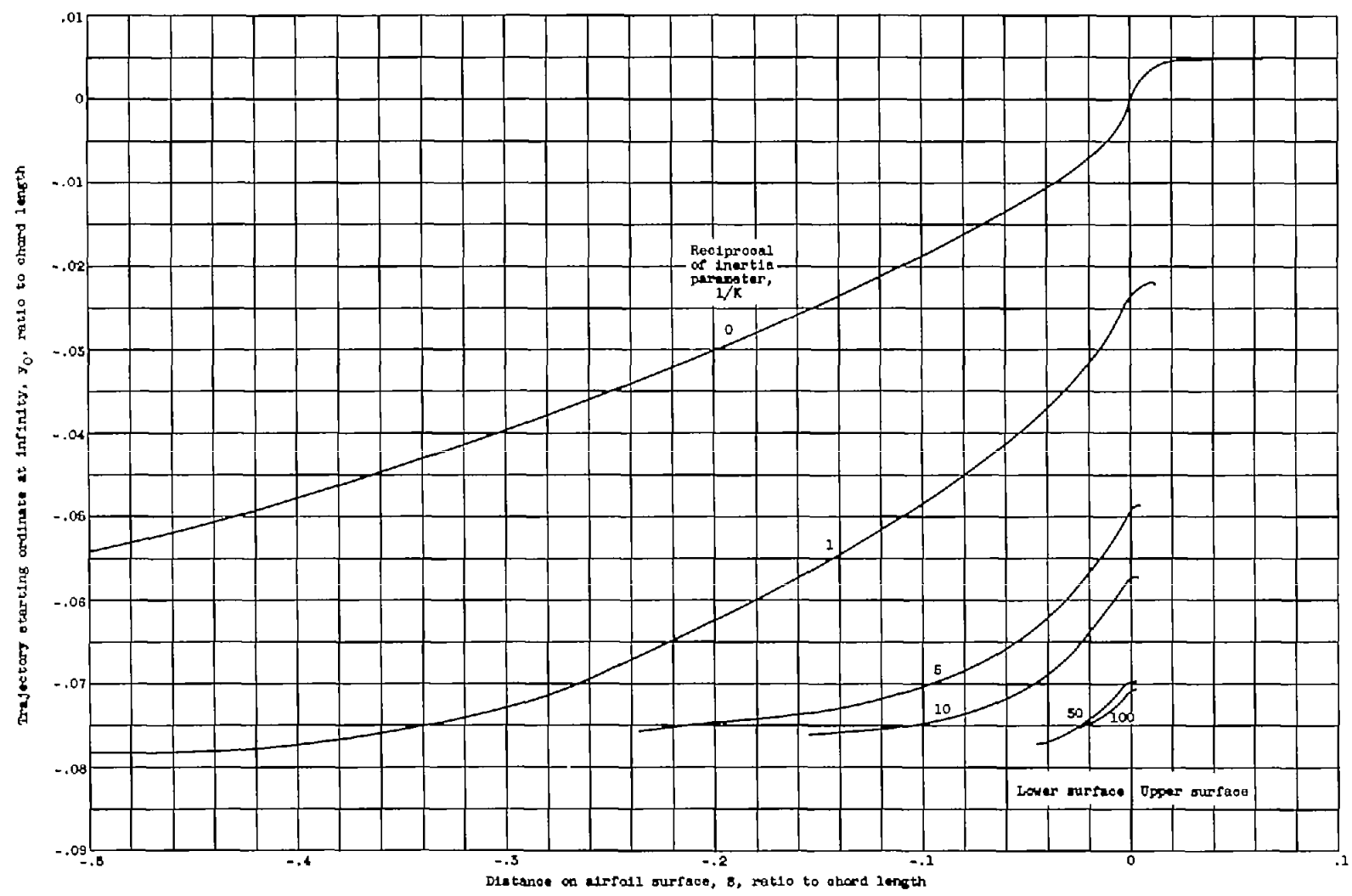


Figure 8. - Continued. Trajectory starting ordinates as function of point of impingement on surface of 85A004 airfoil.

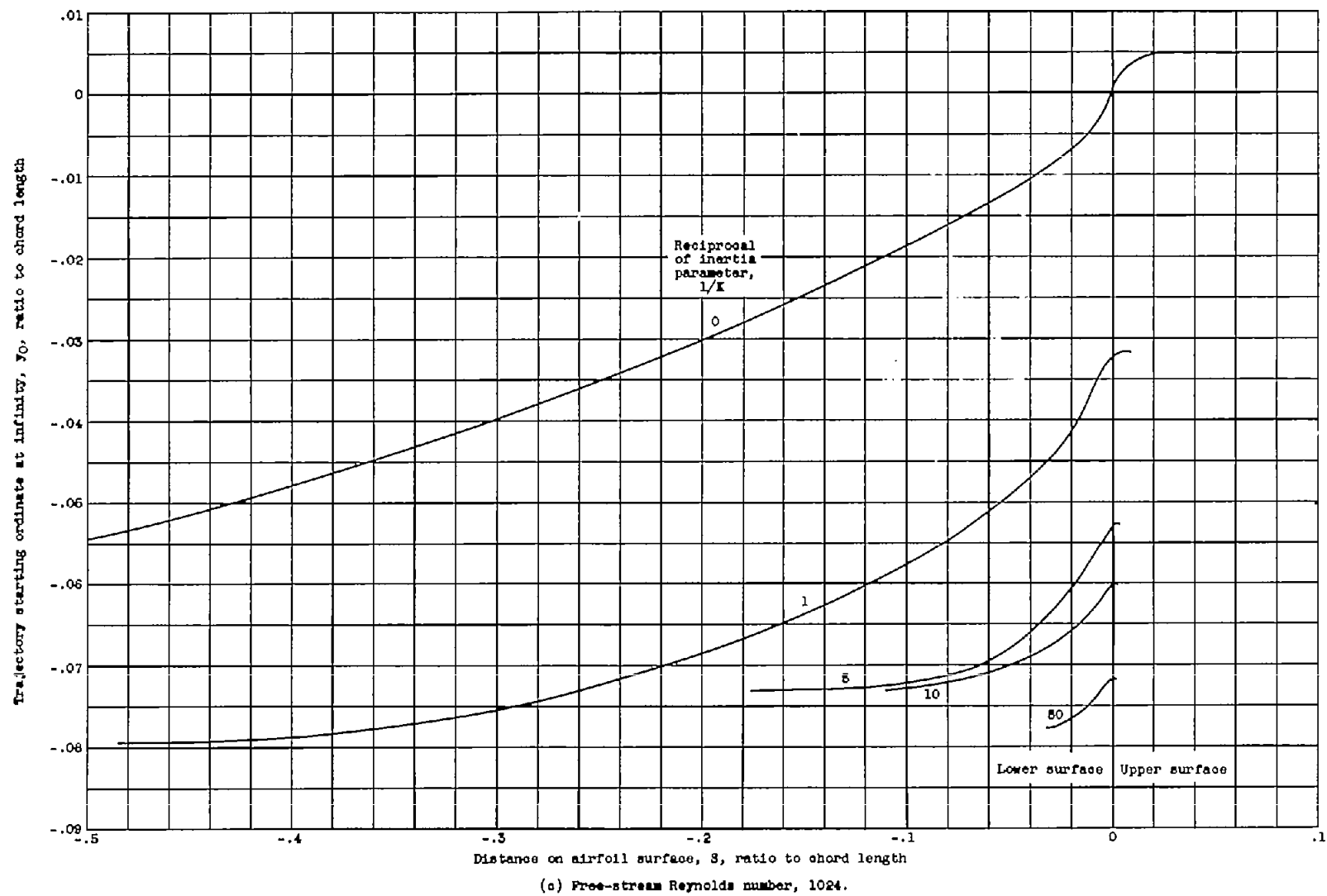
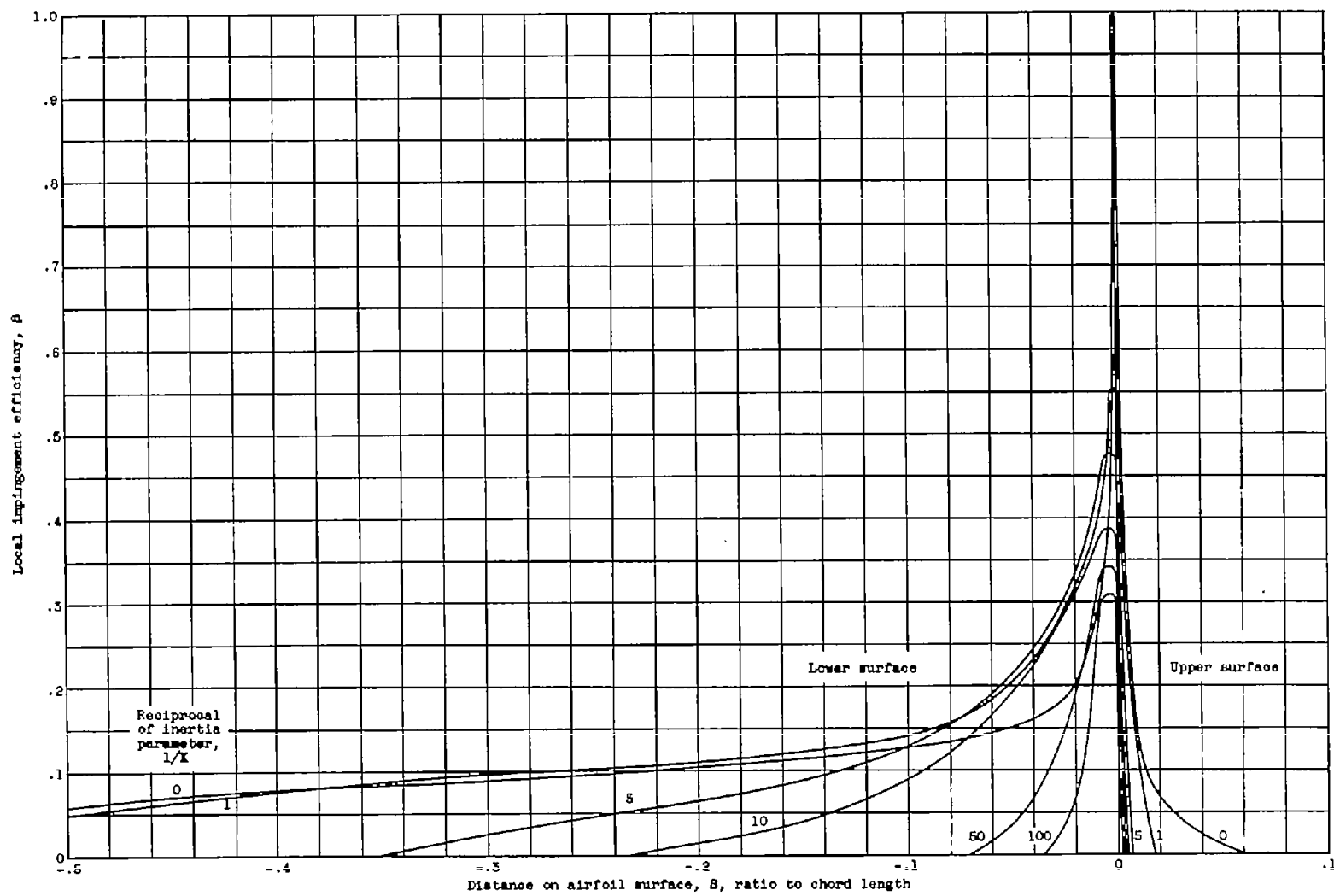
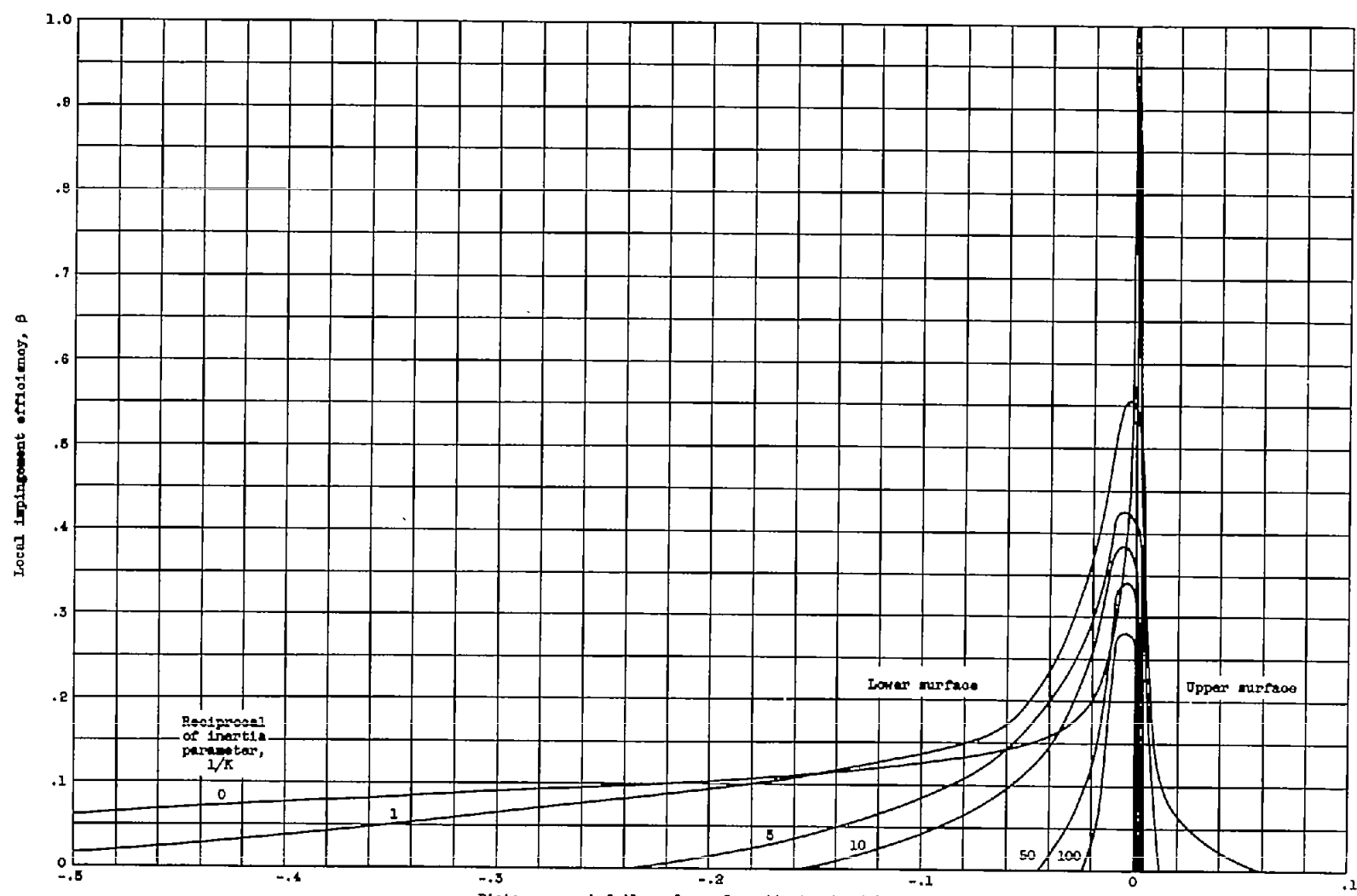


Figure 8. - Concluded. Trajectory starting ordinates as function of point of impingement on surface of 85A004 airfoil.



(a) Free-stream Reynolds number, 16.

Figure 9. - Local impingement efficiency of NACA 85A004 airfoil. Angle of attack,  $4^{\circ}$ .



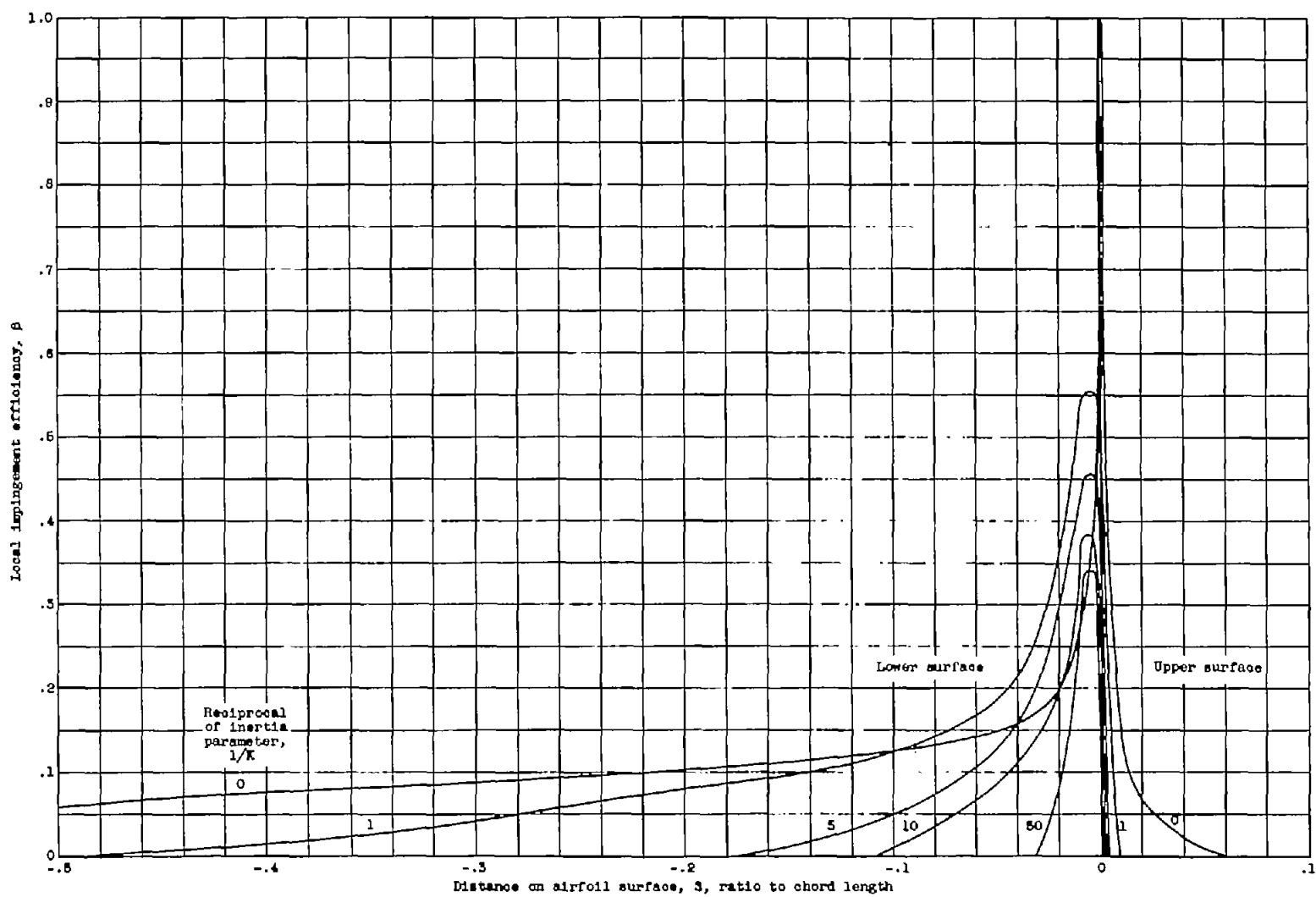


Figure 9. - Concluded. Local impingement efficiency of NACA 65A004 airfoil. Angle of attack,  $4^\circ$ .

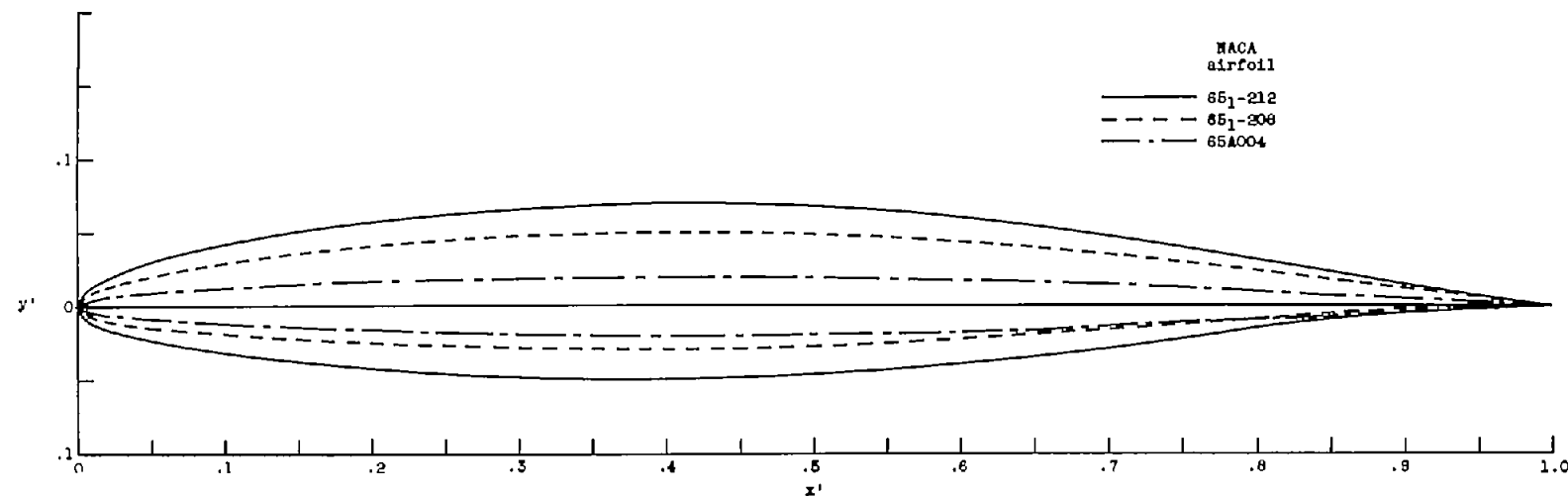


Figure 10. - Comparison of geometric shapes of three airfoils studied.

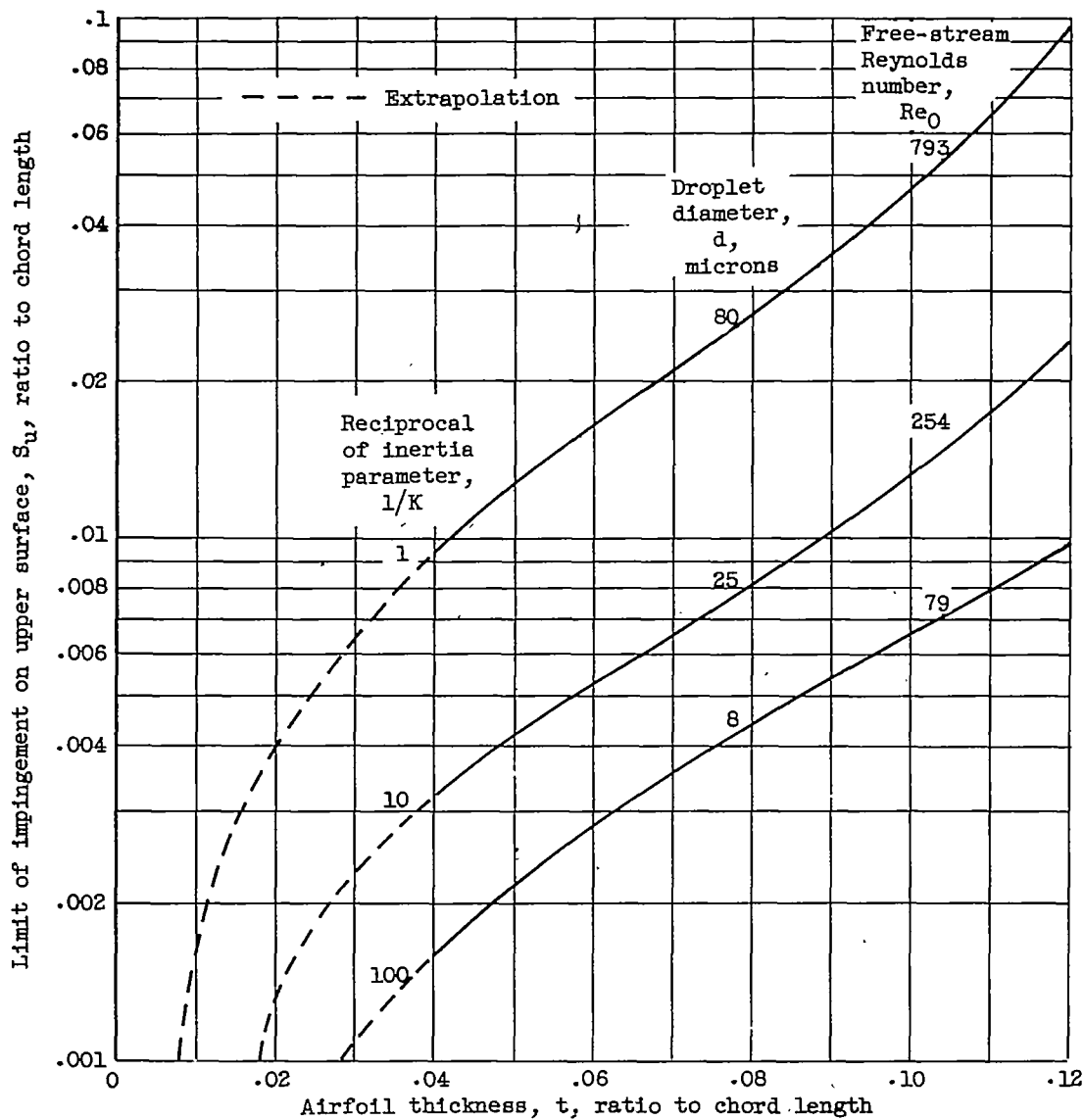
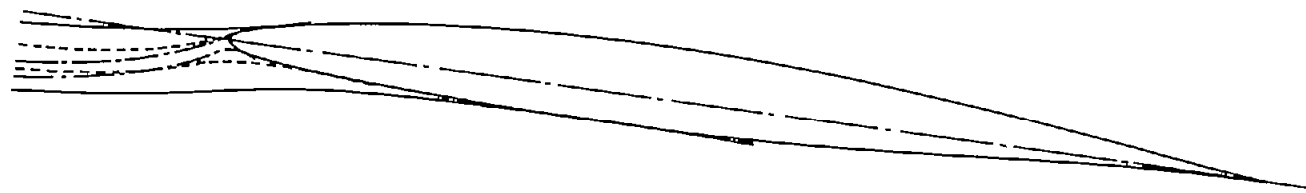


Figure 11. - Limit of impingement on upper surface as function of airfoil thickness ratio. Flight speed, 400 miles per hour; airfoil chord length, 12.5 feet; altitude, 10,000 feet; angle of attack,  $4^\circ$ .

Reciprocal of inertia parameter, $1/K$	Droplet diameter, $d$ , microns	Free-stream Reynolds number, $Re_0$
---	--	--

—	1	80	793
- - -	10	25	254
— — —	100	8	78

(a) NACA 65<sub>1</sub>-212 airfoil.(b) NACA 65<sub>1</sub>-208 airfoil.

(c) NACA 65A004 airfoil.

Figure 12. - Effect of thickness ratio on limit of impingement. Flight speed, 400 miles per hour; chord length, 12.5 feet; altitude, 10,000 feet; angle of attack, 4°.

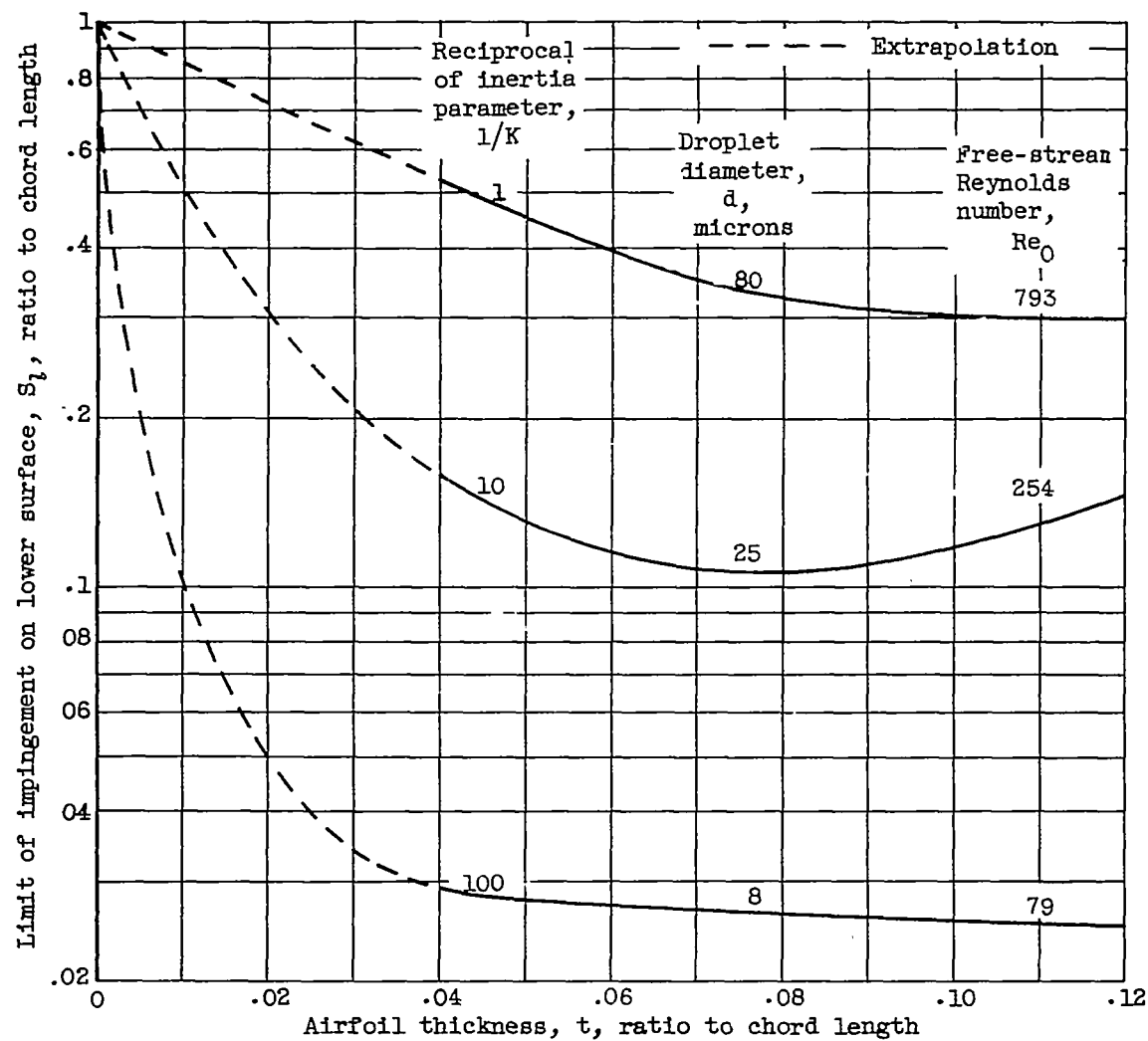


Figure 13. - Limit of impingement on lower surface as function of airfoil thickness ratio. Flight speed, 400 miles per hour; airfoil chord length, 12.5 feet; altitude, 10,000 feet; angle of attack,  $4^\circ$ .

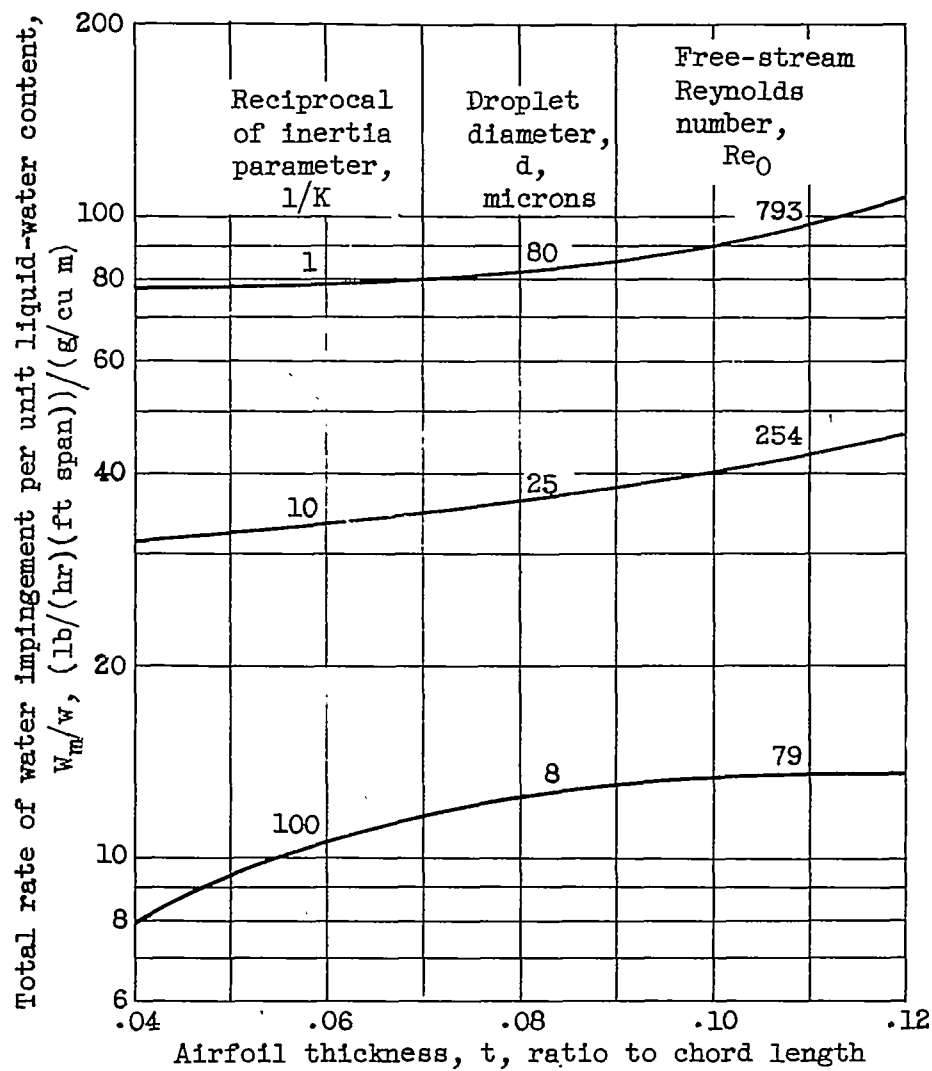


Figure 14. - Rate of water impingement as function of airfoil thickness ratio. Flight speed, 400 miles per hour; airfoil chord length, 12.5 feet; altitude, 10,000 feet; angle of attack,  $4^\circ$ .

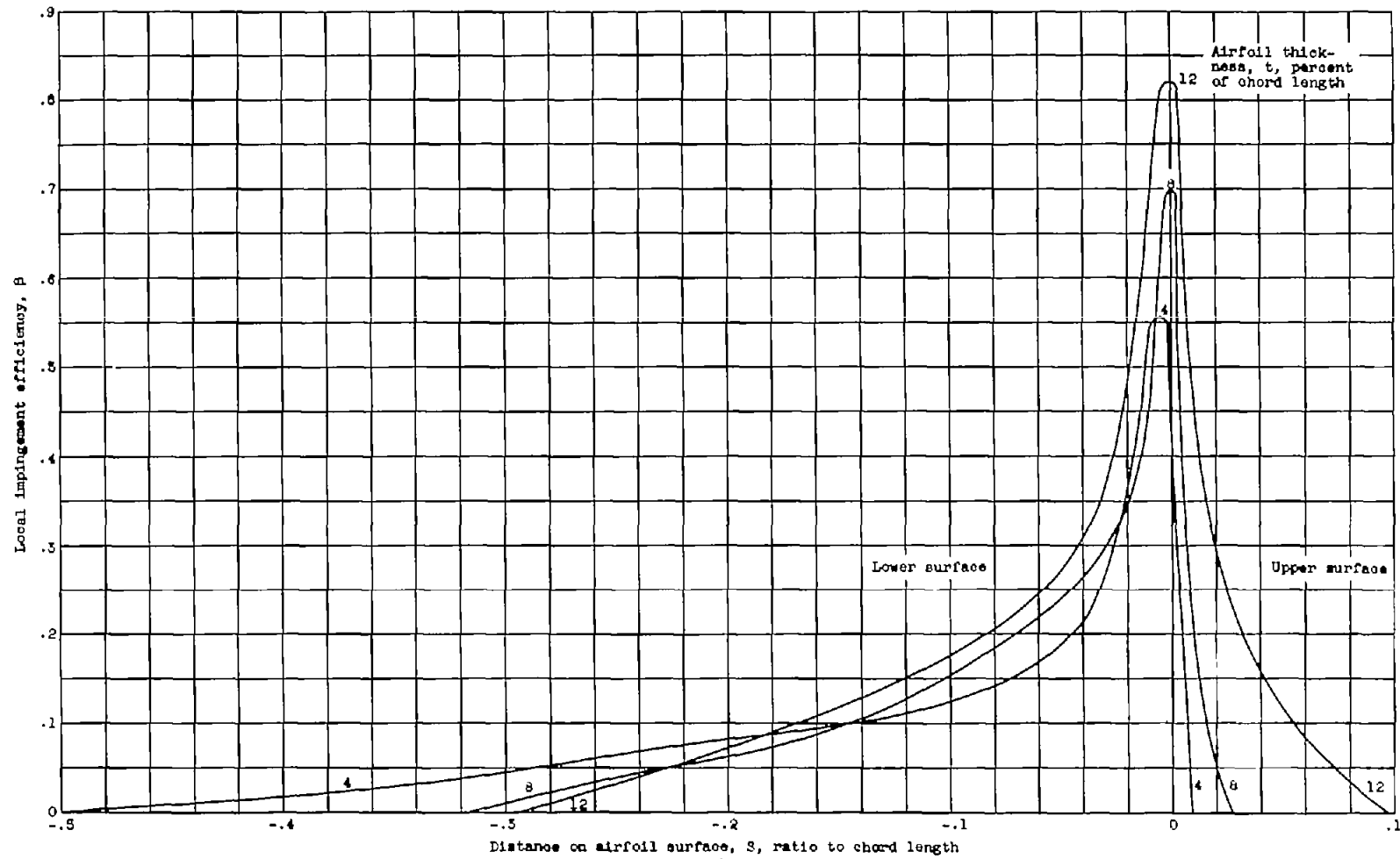


Figure 15. - Local impingement efficiency as affected by airfoil thickness. Flight speed, 400 miles per hour; airfoil chord, 12.5 feet; altitude, 10,000 feet; angle of attack,  $4^{\circ}$ .

NACA TN 3047 - 11-24-63 - 1000

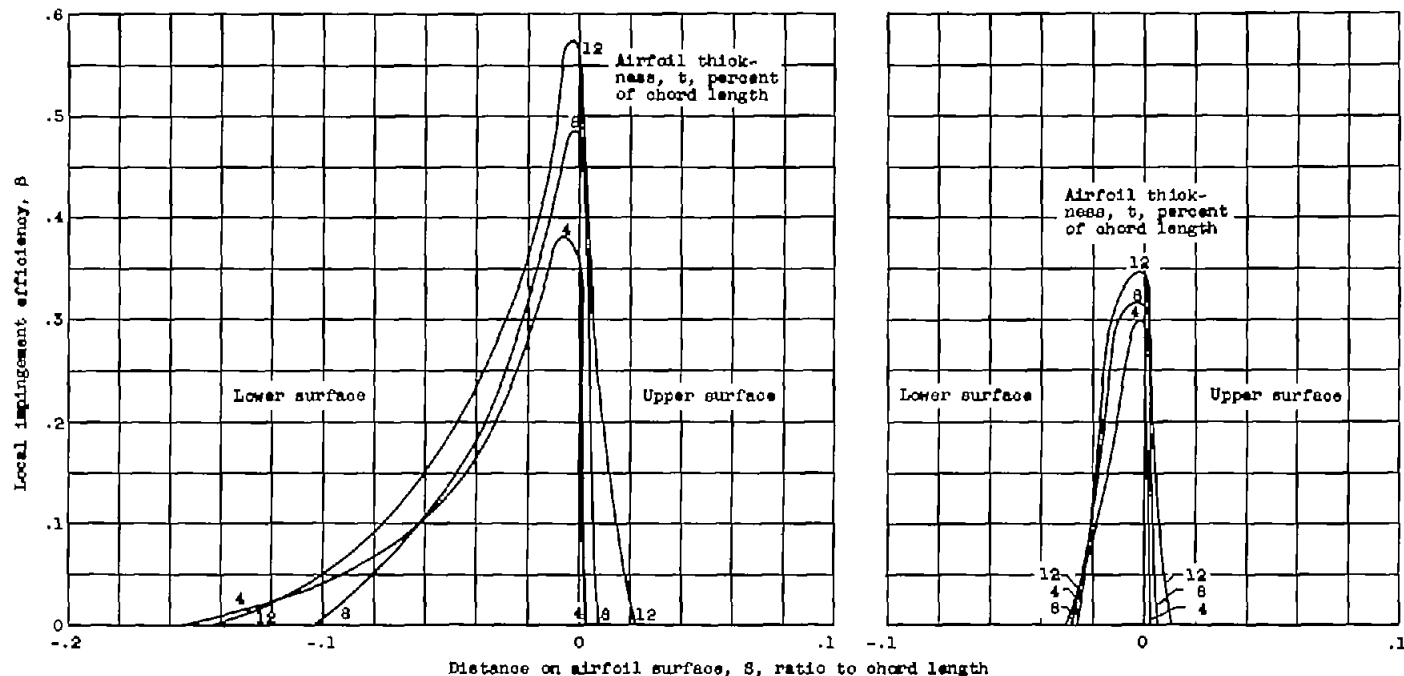


Figure 15. - Concluded. Local impingement efficiency as affected by airfoil thickness. Flight speed, 400 miles per hour; airfoil chord, 12.5 feet; altitude, 10,000 feet; angle of attack,  $4^{\circ}$ .